

## Interacting radiation after Planck and its implications for the Hubble tension

To cite this article: Nikita Blinov and Gustavo Marques-Tavares JCAP09(2020)029

View the article online for updates and enhancements.

#### Recent citations

- The hubble tension as a hint of leptogenesis and neutrino mass generation Miguel Escudero and Samuel J. Witte

- <u>Dark Energy with Phantom Crossing and the H0 Tension</u>
Eleonora Di Valentino *et al* 

- Velocity-dependent interacting dark energy and dark matter with a Lagrangian description of perfect fluids Jose Beltrán Jiménez et al



# IOP ebooks™

Bringing together innovative digital publishing with leading authors from the global scientific community.

Start exploring the collection-download the first chapter of every title for free.

# Interacting radiation after Planck and its implications for the Hubble tension

## Nikita Blinov, $^{a,b}$ and Gustavo Marques-Tavares $^{c,d}$

<sup>a</sup>Fermi National Accelerator Laboratory, Batavia, IL 60510, U.S.A.

<sup>b</sup>Kavli Institute for Cosmological Physics, University of Chicago, Chicago, IL 60637, U.S.A.

<sup>c</sup>Department of Physics and Astronomy, Johns Hopkins University, Baltimore, MD 21218, U.S.A.

<sup>d</sup>Maryland Center for Fundamental Physics, Department of Physics, University of Maryland, College Park, MD 20742, U.S.A.

E-mail: nblinov@fnal.gov, gusmt@umd.edu

Received April 10, 2020 Revised July 16, 2020 Accepted August 9, 2020 Published September 15, 2020

**Abstract.** Standard cosmology predicts that prior to matter-radiation equality about 41% of the energy density was in free-streaming neutrinos. In many beyond Standard Model scenarios, however, the amount and free-streaming nature of this component is modified. For example, this occurs in models with new neutrino self-interactions or an additional dark sector with interacting light particles. We consider several extensions of the standard cosmology that include a non-free-streaming radiation component as motivated by such particle physics models and use the final Planck data release to constrain them. This release contains significant improvements in the polarization likelihood which plays an important role in distinguishing free-streaming from interacting radiation species. Fixing the total amount of energy in radiation to match the expectation from standard neutrino decoupling we find that the fraction of free-streaming radiation must be  $f_{\rm fs} > 0.8$  at 95% CL (combining temperature, polarization and baryon acoustic oscillation data). Allowing for arbitrary contributions of free-streaming and interacting radiation, the effective number of new non-free-streaming degrees of freedom is constrained to be  $N_{\rm fld} < 0.6$  at 95% CL. Cosmologies with additional radiation are also known to ease the discrepancy between the local measurement and CMB inference of the current expansion rate  $H_0$ . We show that including a non-free-streaming radiation component allows for a larger amount of total energy density in radiation, leading to a mild improvement of the fit to cosmological data compared to previously discussed models with only a free-streaming component.

**Keywords:** cosmological parameters from CMBR, cosmology of theories beyond the SM, particle physics - cosmology connection

**ArXiv ePrint: 2003.08387** 

C	ontents	
1	Introduction	1
2	Models of dark radiation	3
	2.1 Non-abelian dark radiation	3
	2.2 Late equilibration of a dark sector	4
3	Impact of interacting radiation	6
	3.1 Boltzmann equations	6
	3.2 Impact on the CMB power spectrum	7
4	Cosmological constraints	9
	4.1 Testing the free-streaming hypothesis for neutrinos	10
	4.2 Models with varying $N_{\text{tot}}$	12
	4.3 Particle physics interpretation	16
5	Conclusion	21
$\mathbf{A}$	Planck TT results	23
В	24	

#### 1 Introduction

Cosmological measurements have become an important probe of Physics Beyond the Standard Model (BSM). Most recently the Planck mission has significantly improved the measurements of the Cosmic Microwave Background (CMB), enabling the precise determination of cosmological parameters and comparison of the standard  $\Lambda$ CDM cosmology to its extensions [1]. The CMB is a particularly powerful probe of BSM scenarios with new light degrees of freedom that are very weakly coupled to the Standard Model (SM), which are challenging to probe directly with terrestrial experiments. These particles, however, are a generic feature of many ultra-violet completions and extensions of the SM including additional neutrinos [2], dark sectors (DS) [3, 4], string axions [5] and axion-like particles [6], and Goldstone bosons [7, 8]. Their cosmological imprints would be a first glimpse into BSM physics, and it therefore constitutes an important science driver of the current and future CMB experiments [9, 10].

New contributions to the energy density of the Universe during recombination from extra relativistic degrees of freedom would lead to observable changes in the CMB spectrum. This extra amount of energy density has been historically parametrized by the number of effective neutrinos,  $N_{\rm eff}$ , with the assumption that it affects the CMB in the same way as neutrinos. There are two important effects on the CMB power-spectrum [11, 12] due to neutrinos. First, they significantly contribute to the expansion rate before matter-radiation equality (MRE), changing the sound horizon and diffusion scales — a purely background cosmology effect, which affects crude features of the CMB power spectrum. Second, the supersonic propagation of neutrino perturbations induces a phase shift on the sound waves in the plasma which manifests as a phase shift in the CMB and baryon acoustic oscillation (BAO) peaks [11, 13].

While  $N_{\rm eff}$  was an appropriate parametrization of any new relativistic degree of freedom for earlier CMB experiments, Planck's measurements are sensitive enough to probe both their contribution to the expansion rate and the evolution of perturbations [13–15]. The latter is very sensitive to the particle nature of the relativistic species. In particular, the phase shift is a direct consequence of the free-streaming nature of neutrinos. In many BSM scenarios, however, the extra radiation interacts with itself or with dark matter, preventing free-streaming and causing the radiation to behave as an ideal relativistic fluid. In these cases  $N_{\rm eff}$  is an inadequate parametrization of the new species.

In this paper we study the impact of Planck's final data release and other cosmological data sets on models with both free-streaming and interacting radiation species with their energy densities parametrized by  $N_{\rm eff}$  and  $N_{\rm fld}$ , respectively. Throughout this work we pay special attention to the impact of the non-free-streaming species on the tensions in the measurements of the local expansion rate  $H_0$  and the amplitude of matter fluctuations  $\sigma_8$ . The discrepancy between local [16, 17] and high-redshift inferences [1, 18–20] of the local expansion rate has a significance of  $\sim 4-5\sigma$  depending on the data sets used (although some local measurements are in better agreement with the CMB [21]). It is well known that additional relativistic degrees of freedom can alleviate this tension by reducing the scale of the sound horizon [22–24]. A multitude of models have been proposed that achieve this by introducing additional energy either in the form of  $N_{\rm eff}$  [25], neutrinos with sizable selfinteractions [26, 27] or interactions with dark matter [28, 29], decaying dark matter [30] or early dark energy [31–34]. Models with non-free-streaming radiation species studied in refs. [13, 35] and in this work can be considered as a limit of the interacting neutrino models, where the self-interactions are sufficiently large (i.e. faster than the Hubble rate) during the times relevant for the CMB. The  $\sigma_8$  tension is milder [1, 36–39], at about  $\sim 2\sigma$ . However models with additional energy at around MRE motivated by  $H_0$  tend to increase  $\sigma_8$  and aggravate the tension. This effect is lessened in models with interacting radiation, enabling it to potentially address both anomalies.

This paper is organized as follows. In section 2 we show how scenarios with new freestreaming or interacting radiation can arise from well-motivated particle physics models. There, we argue that wide variety of free-streaming and interacting species occur naturally in models with non-Abelian hidden sectors, or late equilibration of light particles. These and many other models can be mapped onto an effective fluid description as detailed in section 3; the resulting Boltzmann equations can be easily implemented in a solver such as CLASS [40] or CAMB [41]. We then extend previous analyses of refs. [13, 35] by including the latest data [42] and performing extensive comparisons against the base cosmology and models with only free-streaming species in section 4. The inclusion of the latest data set is essential due to the significant improvements in the treatment of polarization and its relevance for the distinction between interacting and free-streaming radiation, parametrized by  $N_{\rm fld}$  and  $N_{\rm eff}$ , respectively. In addition to models with freely varying  $N_{\text{eff}}$  and  $N_{\text{fld}}$ , we consider subsets of this parameter space motivated by the different scenarios discussed in section 2. In particular, we study the scenario in which  $N_{\rm eff} + N_{\rm fld} = 3.046$  to show that Planck disfavors even one of the neutrino flavors having significant interactions at the time of recombination. This enables us to interpret these results in the context of the specific particle physics models discussed in section 2. We also consider variations of the primordial helium fraction,  $Y_p$ , which allows for much larger radiation densities if one ignores constraints from direct measurements of  $Y_p$ . We summarize our findings and conclude in section 5.

#### 2 Models of dark radiation

In this section we present simple models of dark radiation that lead to different predictions for the contributions to  $N_{\rm eff}$  and to its interacting counterpart  $N_{\rm fld}$ . These models are not meant as a complete set of possibilities, but as examples that motivate searching for a wide range of  $(N_{\rm eff}, N_{\rm fld})$ , which parametrize the cosmic energy density in relativistic degrees of freedom (in addition to the photon).<sup>1</sup> Explicitly, these quantities are normalized such that  $N_{\rm eff} \approx 3.046$  in  $\Lambda {\rm CDM}$  well after neutrino-photon decoupling and electron-positron annihilation (we use the result of ref. [44] — other recent calculations, e.g., refs. [45, 46], give similar values) so the total radiation energy density is

$$\rho_{\rm rad} = \rho_{\gamma} + \rho_{\nu} + \rho_{\rm ds} = \rho_{\gamma} \left[ 1 + \frac{7}{8} (N_{\rm eff} + N_{\rm fld}) \left( \frac{4}{11} \right)^{4/3} \right], \tag{2.1}$$

where  $\rho_{\gamma}$ ,  $\rho_{\nu}$  and  $\rho_{\rm ds}$  are the energy densities in photons, neutrinos and any additional dark sector states. Thus,  $N_{\rm eff}$  and  $N_{\rm fld}$  are completely degenerate at the level of the background cosmology. Following ref. [35] we will often reparametrize these densities in terms of

$$N_{\text{tot}} = N_{\text{eff}} + N_{\text{fld}}, \tag{2.2}$$

$$f_{\rm fs} = N_{\rm eff}/N_{\rm tot},\tag{2.3}$$

so  $N_{\rm tot}$  is the total number of effective relativistic species, and  $f_{\rm fs}$  is the fraction of those that are free-streaming. This parametrization reduces the degeneracy between  $N_{\rm eff}$  and  $N_{\rm fld}$ , enabling a more efficient Monte Carlo exploration of the parameter space. As discussed in the introduction, the degeneracy is also broken by the different evolution of the perturbations in the two fluids due to the presence or absence of self-interactions. Below we discuss how such interactions can naturally arise in particle physics models.

#### 2.1 Non-abelian dark radiation

A simple candidate for dark radiation are gauge bosons of a new non-Abelian group with a very small gauge coupling [47–50]. The smallness of the gauge coupling implies an exponentially small confinement scale, and therefore the relevant degrees of freedom for cosmology are the gauge bosons (dark gluons), which are effectively massless. The gauge structure imposes a minimum amount of self-interactions controlled by the gauge coupling  $g_d$ . Even a tiny gauge coupling is sufficient to make this a perfect fluid, given that the interaction rate is approximately

$$\Gamma_d \sim \alpha_d^2 T_d,$$
(2.4)

where  $\alpha_d = g_d^2/(4\pi)$  and  $T_d$  is the temperature of the dark fluid, which we take to be comparable to the SM temperature. If we require that this interaction is in equilibrium before the photon temperature reaches a keV (and so well before the modes probed by the CMB enter the horizon) we find that

$$\alpha_d \gtrsim 10^{-12} \,. \tag{2.5}$$

This shows that even very small gauge couplings lead to sufficiently large self-interactions to ensure that the dark gluons locally thermalize and thus behave as an ideal fluid.

<sup>&</sup>lt;sup>1</sup>See also [26–29, 43] for other examples of models with an interacting radiation component.

The contribution of dark gluons to  $N_{\rm fld}$  depends on the temperature of the fluid  $T_d$ , and their number  $N_d$ , which is equal to the number of generators of the non-Abelian group (for example, for a dark  ${\rm SU}(N)$ ,  $N_d=N^2-1$ ). The temperature of the dark sector depends on how it interacts with the Standard Model and on details of cosmology at very high temperatures. If it was ever in thermal contact with the SM (and ignoring a possible late reheating of the SM), but decoupled at a temperature  $T_f$ , the dark sector temperature follows from entropy conservation

$$\frac{T_d}{T_\gamma} = \left[ \frac{g_{*S}(T_\gamma)}{g_{*S}(T_f)} \right]^{1/3},\tag{2.6}$$

where  $g_{*S}$  is the effective number of (entropy) relativistic species including the neutrino contribution. Using eq. (2.1) this leads to

$$N_{\rm fld} = \frac{8}{7} \left(\frac{11}{4}\right)^{4/3} \left(\frac{T_d}{T_{\gamma}}\right)^4 N_d. \tag{2.7}$$

Note that thermal equilibrium at early times implies a minimum dark sector temperature

$$\frac{T_d}{T_{\gamma}} \gtrsim 0.33 \implies N_{\text{fld}} \gtrsim 0.054 N_d \,, \tag{2.8}$$

where we evaluated eq. (2.6) at  $T_f \gg 100$  GeV and  $T_\gamma \sim 1$  eV. This shows that even the simplest SU(2) non-Abelian dark sector ( $N_d=3$ ) implies  $N_{\rm fld} \gtrsim 0.16$  (in the absence of non-SM entropy injections at temperatures below the weak scale).

In the above model of a decoupled DS,  $N_{\rm eff} = 3.046$  and  $N_{\rm fld}$  can take on any positive value. Next, we consider a model where instead  $N_{\rm tot} = 3.046$  is fixed, but  $f_{\rm fs}$  is allowed to vary.

#### 2.2 Late equilibration of a dark sector

A dark sector could come into equilibrium with the Standard Model neutrinos after Big Bang Nucleosynthesis (BBN) as considered in [4, 51, 52]. This possibility has a number of interesting features. In particular it predicts no deviations in  $N_{\rm tot}$  during BBN, and, as we will discuss, can decrease the neutrino contribution to  $N_{\rm tot}$  at CMB, effectively replacing it with new BSM particles. We will refer to this scenario as "late equilibration".

A simple model that realizes this scenario involves adding a new massive scalar  $\phi$  that directly couples to neutrinos  $\nu$  via

$$\mathcal{L} \supset \frac{1}{2} \lambda_{\nu} \phi \nu \nu + \text{h.c.}, \tag{2.9}$$

where  $\lambda_{\nu}$  is a dimensionless coupling constant (neutrino flavor indices are suppressed). Such interactions are characteristic of Majoron models where  $\phi$  is part of the sector that generates neutrino masses [53]. The scalar will come into equilibrium with the neutrinos through inverse decays  $\nu\nu \leftrightarrow \phi$  at a temperature [4, 53, 54]

$$T_{\phi}^{\text{eq}} \sim \left(\frac{\lambda_{\nu}^2 m_{\phi}^2 M_{\text{Pl}}}{8\pi}\right)^{1/3},$$
 (2.10)

where we have assumed  $T_{\phi} > m_{\phi}$  (inverse decay also requires  $m_{\phi} > 2m_{\nu}$ , where  $m_{\nu}$  is the mass of the neutrino(s) interacting with  $\phi$ ). Equilibration conserves energy, so as long as

 $m_{\phi} < T_{\phi} <$  MeV (i.e. equilibration occurs after neutrino-photon decoupling) and the initial DS temperature is lower than that of the SM, the total amount of energy in relativistic species remains approximately constant, i.e.  $N_{\rm eff} + N_{\rm fld} \approx 3$ , and the successful prediction standard BBN remain [54]. The forward and inverse  $\phi$  decays that enforce chemical equilibrium can also tightly couple the  $\phi$  and neutrino fluids, preventing free-streaming. The kinematics of the  $1\leftrightarrow 2$  processes suppress the requisite momentum isotropization rate by an additional factor of  $(m_{\phi}/T)^2$  compared to the decay/production rate discussed above [51, 55]. As a result, the temperature at which neutrino stops free-streaming,  $T_{\phi}^{\rm nfs}$ , is parametrically smaller than the equilibration temperature:

$$T_{\phi}^{\text{nfs}} \sim \left[ \left( T_{\phi}^{\text{eq}} \right)^3 m_{\phi}^2 \right]^{1/5}.$$
 (2.11)

If this kinetic equilibrium persists through recombination (i.e.  $m_{\phi} \lesssim 0.1$  eV), this minimal scenario predicts

$$N_{\rm tot} = N_{\rm eff} + N_{\rm fld} \approx 3, \qquad (2.12)$$

and the fraction of free-streaming radiation  $f_{\rm fs}$ 

$$f_{\rm fs} = N_{\rm eff}/N_{\rm tot} \le 1 \tag{2.13}$$

depends on how many neutrino flavors  $\phi$  interacts with (i.e. the flavor structure of eq. (2.9)). The limits  $f_{\rm fs} \to 0$  and  $f_{\rm fs} \to 1$  correspond to  $\phi$  interacting with all or none of the neutrino flavors, respectively.<sup>2</sup> The  $f_{\rm fs} \to 0$  scenario has been extensively studied under different assumptions about the temperature scaling of the reaction rate responsible for the  $\phi$ - $\nu$  interactions [27, 43, 56–61]. The  $N_{\rm fld}$  model simply corresponds to the limit in which the  $\phi$ - $\nu$  (or the  $\nu$ - $\nu$  scattering implied by eq. (2.9)) interactions are faster than Hubble for all scales probed by the observed CMB. Interestingly, couplings  $\lambda_{\phi}$  and masses  $m_{\phi}$  implied by late equilibration are small enough to (mostly) avoid stringent cosmological and laboratory bounds that constrain new neutrino interactions [62].

The scalar  $\phi$  can also be a portal to a richer DS if  $\phi$  couples to additional states more strongly than to neutrinos. Then  $\phi$ - $\nu$  equilibration also brings those extra states into equilibrium, sharing the total energy density between the neutrinos and the DS proportionally to the number of degrees of freedom in each sector. If the number of DS states is much larger than 3, most of the energy will be in these new particles rather than neutrinos. This is a realization of the "neutrinoless universe" [63], where the non-photon energy density is almost entirely in non-free-streaming species, i.e.  $N_{\rm tot} \approx N_{\rm fld}$  and  $f_{\rm fs} \approx 0$ . If some of DS states are massive and at some point become non-relativistic, their entropy is shared among the remaining states, increasing their temperature relative to photons and thereby increasing  $N_{\rm tot}$ .

A concrete realization of the above ideas can be constructed by assuming that  $\phi$  couples to N light Weyl fermions  $\psi_i$ :

$$\mathcal{L} \supset \frac{1}{2}\phi \sum_{i=1}^{3} \lambda_{\nu_i}\nu_i\nu_i + \frac{1}{2}\lambda_{\psi}\phi \sum_{i=1}^{N} \psi_i\psi_i + \text{h.c.}, \qquad (2.14)$$

where we took the  $\phi$  coupling to dark radiation to be the same for all species, but allowed for mass eigenstate-dependence of  $\lambda_{\nu}$ . Assuming  $\lambda_{\psi} \gg \lambda_{\nu}$ , as soon as  $\phi$  enters thermal and

<sup>&</sup>lt;sup>2</sup>If the  $f_{\rm fs} \to 0$  regime is obtained via decays and inverse decays  $\nu\nu \leftrightarrow \phi$ , then we must demand  $m_{\phi} \gtrsim 2m_{\nu_3} > 0.1$  eV, so the treatment of  $\phi$  as an additional radiation species may break down near recombination.

chemical equilibrium with neutrinos through inverse decay  $\nu\nu \leftrightarrow \phi$ , the dark radiation will also enter equilibrium with the neutrinos via decays of  $\phi \leftrightarrow \psi\psi$ . After equilibration, the temperature of the combined  $\nu$ +DS bath is determined from energy conservation [53, 54]:

$$\frac{T_{\nu+\text{ds}}}{T_{\gamma}} = \left(\frac{4}{11}\right)^{1/3} \left(\frac{N_{\nu}}{N_{\nu} + N'}\right)^{1/4},\tag{2.15}$$

where  $N_{\nu}$  is the number of neutrino mass eigenstates that interact with  $\phi$  (corresponding to the number of non-negligible couplings  $\lambda_{\nu_i}$ ) and N'=N+(4/7) counts the contributions of  $\psi_i$  and  $\phi$ ; we also assumed that before equilibration the DS temperature is  $T_{\rm ds}/T_{\gamma} \lesssim 0.5$ . In the limit  $N' \to 0$  we recover the standard result for neutrino temperature well after  $e^{\pm}$  annihilation. If  $N' \gg N_{\nu}$ , however, we see that  $\rho_{\nu}/(\rho_{\phi}+\rho_{\psi})=N_{\nu}/N'$  and the interacting neutrinos contribute negligibly compared to the DS states. One can check using the definition of eq. (2.1) that the temperature in eq. (2.15) guarantees that  $N_{\rm tot} \approx 3$ . This continues to hold as long as all particles in equilibrium are relativistic. If a number  $N_h$  of "heavy"  $\psi$  states become non-relativistic and decay or annihilate into the other lighter states, entropy conservation leads to an increase of  $T_{\nu+{\rm ds}}/T_{\gamma}$  and a corresponding increase in  $N_{\rm tot}$  [53, 54]:

$$N_{\text{tot}} \approx 3 - N_{\nu} + N_{\nu} \left( \frac{N_{\nu} + N'}{N_{\nu} + N' - N_{b}} \right)^{1/3}$$
 (2.16)

Thus, multiple "freeze-out" events can further increase the total radiation density compared to photons. Depending on N, couplings and masses of the DS states, this scenario can realize a wide range of  $N_{\rm eff}$  and  $N_{\rm fld}$ , or just the subspace with  $N_{\rm tot} \approx 3$ . Note that in this scenario, even if  $m_{\phi} > {\rm keV}$ , and therefore  $\phi$  is not directly relevant for the physics of the CMB, the dark radiation can still be sufficiently self-interacting through off-shell  $\phi$  exchanges to be treated as a perfect fluid during the time relevant for CMB measurements (because  $\lambda_{\psi}$  can be much larger than  $\lambda_{\nu}$ ), while the neutrinos would be free-streaming (because the  $\nu$ - $\nu$  scattering rate through off-shell  $\phi$  would be too small). The alternative possibility of dark sector self-interactions falling out of equilibrium during times relevant for the CMB has been considered in ref. [64].

#### 3 Impact of interacting radiation

We work with the perturbed Friedmann-Robertson-Walker spacetime [65, 66]

$$ds^{2} = a^{2}(\eta) \left[ -(1+2A)d\eta^{2} + (\delta_{ij} + 2h_{ij})dx^{i}dx^{j} \right]$$
(3.1)

where  $\eta$  is the conformal time, and  $A = \Psi$  and  $h_{ij} = -\Phi$  in conformal Newtonian gauge (A = 0 and  $h_{ij} = h\hat{k}_i\hat{k}_j/2 + 3\eta_L(\hat{k}_i\hat{k}_j - \delta_{ij}/3)$  in synchronous gauge) are the metric perturbations in Fourier space. We follow the notation of ref. [30] below, which closely resembles that of the Boltzmann solver CLASS [40].<sup>3</sup>

#### 3.1 Boltzmann equations

The evolution equations for the interacting radiation fluid follow from conservation of the energy-momentum tensor [65]. The background equation is

$$\rho' + 4\left(\frac{a'}{a}\right)\rho = 0, (3.2)$$

<sup>&</sup>lt;sup>3</sup>We used  $\eta_L$  for the synchronous gauge metric perturbation instead of  $\eta$  used in refs. [65, 66] to distinguish it from the conformal time.

where primes denote derivatives with respect to the conformal time  $\eta$ ; the solution is  $\rho(\eta) = \rho_i a(\eta)^{-4}$ , the same as for a free-streaming species. We define  $\rho_i$  in terms of  $\Omega_{\rm fld} = \rho_i/\rho_{\rm crit}$ , the fluid density today normalized to the critical density, which, in turn, is defined by  $N_{\rm fld}$ :

$$\Omega_{\rm fld} = \frac{7}{8} N_{\rm fld} \left(\frac{4}{11}\right)^{4/3} \Omega_{\gamma}. \tag{3.3}$$

The perturbation equations in conformal time are

$$\delta' = -\frac{4}{3}(\theta + \mathbf{m}_{\text{cont}}) \tag{3.4}$$

$$\theta' = \frac{1}{4}k^2\delta + \mathbf{m}_{\text{Euler}} \tag{3.5}$$

where  $\delta$  and  $\theta$  are the density and velocity perturbations (see, e.g., ref. [65]) and  $\mathbf{m}$  are gauge-dependent quantities appearing in continuity and Euler equations; their values in the Newtonian and synchronous gauges are

	Newtonian	Synchronous
$\mathbf{m}_{\mathrm{cont}}$	$-3\Phi'$	h'/2
$\mathbf{m}_{\mathrm{Euler}}$	$k^2\Psi$	0

Combining eqs. (3.4) and (3.5) gives

$$\delta'' + \frac{1}{3}k^2\delta = -\frac{4}{3}(\mathbf{m}_{\text{Euler}} + \mathbf{m}'_{\text{cont}}),\tag{3.6}$$

which makes it clear that disturbances in this fluid propagate with the sound speed  $1/\sqrt{3}$  (the equivalent expression for free-streaming species depends on shear and higher moments of the phase space distribution preventing the same interpretation of the  $k^2\delta/3$  term).

The presence of non-free-streaming radiation also changes the initial conditions for the adiabatic perturbations. In particular in conformal Newtonian gauge the initial condition for the gravitational potential is [11, 65]

$$\Psi(\eta_i) = -\frac{2\zeta}{3(1 + 4R_{\nu}/15)},\tag{3.7}$$

where  $\zeta$  is the comoving curvature perturbation fixed by inflation,  $R_{\nu} = \rho_{\rm fs}/\rho_{\rm tot}$  is the ratio of energy density in free-streaming species to the total energy density. From that we see that introducing an interacting radiation component lowers  $R_{\nu}$ , and thus increases the amplitude of the potential (for fixed  $\zeta$ ).

#### 3.2 Impact on the CMB power spectrum

The impact of free-streaming and interacting radiation has been extensively studied [11–13, 67]. Here we summarize the main physical quantities highlighted in these works which will help us to interpret the results of the following sections.

At the background level, free-streaming and interacting radiation contribute to the expansion rate of the universe, affecting the physical distances that shape the power spectrum. In particular, key roles are played by the sound horizon  $r_s$ , the photon diffusion scale  $r_d$  and the angular diameter distance to last scattering  $D_A$ .

The comoving sound horizon  $r_s$  is

$$r_s = \int_0^{t_d} \frac{dt}{a(t)} c_s(a) = \int_0^{a_d} da \frac{c_s(a)}{a^2 H(a)},$$
(3.8)

where  $c_s$  is the baryon-photon sound speed and  $t_d$  ( $a_d$ ) time (scale factor) at which the baryons decouple from the radiation.<sup>4</sup> This is an early-time quantity that depends on the contents of the universe prior to recombination through the Hubble expansion rate H(a). The sound horizon determines the spacing of the peaks in the CMB power spectrum as we discuss below.

Temperature fluctuations in the baryon-photon plasma are exponentially damped at small scales due to photon diffusion induced by their non-zero mean free path. The characteristic comoving damping scale  $r_d$  is given by [68-70]

$$r_d^2 = \pi^2 \int_0^{a_d} \frac{da}{a^3 x_e n_e H \sigma_T} \left[ \frac{R^2 + 16(1+R)/15}{6(1+R)^2} \right], \tag{3.9}$$

where  $x_e(a)$  is the free electron fraction,  $\sigma_T$  the Thomson scattering cross-section and  $R=3\rho_b/(4\rho_\gamma)$ . Modes that are physically smaller than this scale have exponentially suppressed power. This equation highlights two important points. First, the response of  $r_d$  to additional contributions to the energy density during the radiation era (entering through H) is weaker compared to  $r_s$  (due to the square root in the definition of  $r_d$ ) [12, 23, 24]; this ensures that  $r_s/r_d$  changes if the early-time energy content is modified. Second, eq. (3.9) makes explicit a degeneracy between additional radiation and  $x_e$ . In particular, close to recombination  $x_e \propto (1-Y_p)$ , so the effects of larger energy densities on the damping scale can be partly compensated by varying  $Y_p$  [12]. In the standard cosmology  $Y_p$  is not a free parameter, since it is completely determined by the baryon and neutrino densities through standard Big Bang Nucleosynthesis.

Neither the sound horizon, nor the photon diffusion scale are directly observable. Instead, observations constrain the projection of these length scales onto the sky which additionally depends on the (comoving) angular diameter distance to the surface of last scattering,  $D_A$ :

$$D_A = \int_{a_A}^{1} \frac{da}{a^2 H(a)}. (3.10)$$

The angular diameter distance is a late-time quantity, i.e., a function of the energy content after recombination. However, the power spectrum is sensitive to the scale of matter-radiation equality through the radiation driving effect, which amplifies the modes that enter the horizon during radiation domination [71]. This results in a large positive correlation between the matter density  $\omega_m$  and the amount additional radiation, as the data requires the redshift of matter-radiation equality to be approximately fixed [12]. Since  $D_A$  depends sensitively on  $\omega_m$ , additional radiation modifies this distance scale indirectly.

The projected quantities imprinted onto the CMB power spectrum are  $r_s/D_A$  and  $r_d/D_A$ . As we describe below,  $r_s/D_A$  determines the angular scale of the peaks in the CMB power spectrum, which are measured with exquisite precision. This tight constraint ensures that a decrease of  $r_s$  due to additional radiation must be compensated by a decrease

<sup>&</sup>lt;sup>4</sup>We will not distinguish between the end of the drag epoch and last scattering, which lead to sound horizons that are slightly different. Importantly, their dependence on model parameters is identical. See ref. [24] for a recent discussion.

in  $D_A$  which is achieved by increasing  $H_0$ . This is why additional radiation tends to ameliorate the Hubble tension. However, since this extra energy density necessarily modifies  $r_s/r_d$  as described above, the CMB constraint on the angular diffusion scale  $r_d/D_A$  prevents large departures from  $N_{\rm tot} \approx 3$ . Note that the effects described so far stem from variations of the background cosmology which do not distinguish free-streaming from interacting radiation.

The difference between free-streaming and interacting radiation arises at first order in perturbation theory. As discussed in refs. [11, 13], the supersonic propagation of free-streaming radiation induces a phase shift into the CMB power spectrum. The peak positions are shifted by (in the flat sky approximation)

$$\ell_p \approx n(\pi - \delta\varphi) \frac{D_A}{r_s},\tag{3.11}$$

where for modes with  $kr_s \gg 1$  the phase shift  $\delta \varphi$  is [11, 13]

$$\delta \varphi \approx 0.191 \pi \left( \frac{\rho_{\rm fs}}{\rho_{\rm rad}} \right),$$
 (3.12)

where  $\rho_{\rm fs}$  is the energy density of free-streaming species. Even if the free-streaming energy density is fixed, additional contributions to non-free-streaming components will lower this phase shift.

Another effect from interacting radiation is to reduce the impact of the free-streaming component on the radiation driving envelope of the CMB. Modes that enter the horizon during radiation domination get a boost in their amplitude due to the rapidly decaying gravitational potential, leading to an increase in the oscillation amplitude proportional to the gravitational potential at horizon crossing [68, 72]. Free-streaming components reduce the size of the gravitational potential with respect to the primordial curvature perturbations (as seen from eq. (3.7)). Introducing an interacting component reduces  $f_{\rm fs}$ , enhancing power at small scales (compared to an  $N_{\rm eff}$  model with the same  $N_{\rm tot}$ ). This effect can partly compensate for the increased effect of diffusion damping, and therefore we expect slightly weaker CMB constraints on  $N_{\rm fld}$  models compared to the ones with extra  $N_{\rm eff}$ .

In the following section we discuss how the correlations implied by the above discussion are realized in the Monte Carlo results, and their implications for the cosmological tensions.

#### 4 Cosmological constraints

In this section we study the cosmological constraints on three different extensions of  $\Lambda$ CDM:

- $(N_{\rm tot} = 3.046, f_{\rm fs})$ : we fix  $N_{\rm tot}$  to the expected  $\Lambda {\rm CDM}$  value 3.046 and allow  $f_{\rm fs}$  to vary with flat prior in the range  $0 \le f_{\rm fs} \le 1$ .
- $(N_{\rm eff} = 3.046, N_{\rm fld})$ : we fix  $N_{\rm eff}$  to the expected  $\Lambda {\rm CDM}$  value 3.046 and allow  $N_{\rm fld}$  to vary with flat prior in the range  $0 \le N_{\rm fld} \le 2$ .
- $(N_{\rm eff}, N_{\rm fld})$ : we allow  $N_{\rm tot} = N_{\rm eff} + N_{\rm fld}$  and  $f_{\rm fs} = N_{\rm eff}/N_{\rm tot}$  to vary independently with flat priors in the range  $2 \le N_{\rm tot} \le 4.5$  and  $0 \le f_{\rm fs} \le 1$ .

At the end of this section we will also explore the known degeneracy between  $Y_p$ , the primordial <sup>4</sup>He fraction, and extra radiation [12], by allowing  $Y_p$  to vary independently of its standard primordial nucleosynthesis prediction. We will present results that do not include any prior on  $Y_p$  and evaluate the impact of imposing a prior from direct measurements.

In order to obtain constraints on the parameters of these models we included the equations. (3.4), (3.5) for an interacting radiation species in the Boltzmann code CLASS [40] interfaced with MontePython 3.2<sup>5</sup> [73] using combinations of the following likelihoods:

- Planck TT: full Planck 2018 TT likelihood, low- $\ell$  polarization likelihood (lowE) and lensing likelihood as described in ref. [42].
- *Planck* TT, TE, EE: full Planck 2018 TT, TE and EE likelihoods and lensing likelihood as described in ref. [42].
- BAO: BOSS DR12 BAO results [74] (both the BAO and full-shape results); small z BAO measurements from the 6dF [75] and BOSS MGS [76] catalogs.
- $H_0$ : local  $H_0$  measurement (with a simple Gaussian likelihood parametrized by  $H_0 = 74.03 \pm 1.42 \text{ km/s/Mpc}$ ) from ref. [16].

In addition to the new parameters associated with each model, we use flat priors for the  $\Lambda$ CDM parameters ( $\theta_s, \omega_b, \omega_c$ ,  $\ln 10^{10} A_s, n_s, \tau$ ), where  $\omega_i = \Omega_i h^2$ . These parameters are described in, e.g., ref. [1]. Here we use  $\Lambda$ CDM to refer to the standard cosmological model with massless neutrinos to facilitate comparisons against models with arbitrary radiation content; non-zero neutrino masses tend to worsen the tension of CMB data with the local measurement of  $H_0$  [1], and would make the preference for additional radiation even more dramatic. The results are obtained by running 8 chains for each model until the Gelman-Rubin convergence criterion  $R-1 \ll 0.05$  is satisfied for all of the parameters [77, 78]. We compare the goodness-of-fit of various models via  $\chi^2$  evaluated at the maximum of the posterior distribution, which is found numerically using multiple restarts of scipy [79] Nelder-Mead and iminuit [80, 81] minimization. We present our main findings in the next subsections; additional results including different data sets and the full 2d posterior distributions are collected in appendices A and B.

#### 4.1 Testing the free-streaming hypothesis for neutrinos

We first present results for the model with  $N_{\rm tot}=3.046$  with different combinations of likelihoods in table 1, where in addition to the parameters scanned by MontePython we also show the derived parameters  $(H_0, r_s^{\rm drag}, \sigma_8)$ , where  $r_s^{\rm drag}$  is the sound horizon at the end of the baryon drag epoch. We see that even using only the TT likelihood there are already stringent constraints on the fraction of radiation that is not free-streaming:  $f_{\rm fs}>0.74$  (at 95.4% confidence). When we include full polarization information and the BAO likelihood we find  $f_{\rm fs}>0.80$  (at 95.4% confidence), which shows that not even one of the neutrino flavors can have significant interactions during recombination. This is in agreement with a previous analysis of 2015 data by the Planck collaboration which used a generalized fluid description to capture these different possibilities [82]. The posterior distribution for  $f_{\rm fs}$  is shown in figure 1, where we compare the effect of using only the TT likelihood with using

<sup>&</sup>lt;sup>5</sup>We found that the initial implementation of the 2018 Planck likelihoods did not include a Gaussian prior on a linear combination of parameters accounting for background from the kinetic and thermal Sunayev-Zeldovich effects [42]. These backgrounds contribute to the high- $\ell$  part of the CMB power spectrum and are therefore somewhat degenerate with the impact of extra radiation on the damping tail. Including this prior had a mild ( $\lesssim 0.5\sigma$ ) effect on parameter means, but a more significant effect on the best-fit values of  $\chi^2$  as the nuisance parameters were driven to their boundaries without this prior. The Gaussian prior is included in our work and has been implemented in MontePython 3.3.

	Planck TT	Planck TT, TE, EE	Planck TT, TE, EE + BAO
$100\theta_s$	$1.0427^{+0.0006}_{-0.00097}$	$1.0428^{+0.00054}_{-0.00073}$	$1.0428^{+0.00049}_{-0.00076}$
$100\Omega_b h^2$	$2.226^{+0.023}_{-0.025}$	$2.244^{+0.017}_{-0.015}$	$2.244^{+0.014}_{-0.014}$
$\Omega_c h^2$	$0.1207^{+0.0018}_{-0.0018}$	$0.1201^{+0.0012}_{-0.0012}$	$0.11996^{+0.00093}_{-0.00096}$
$\ln 10^{10} A_s$	$3.023^{+0.021}_{-0.017}$	$3.029^{+0.017}_{-0.018}$	$3.03^{+0.019}_{-0.016}$
$n_s$	$0.9561^{+0.009}_{-0.0064}$	$0.9589^{+0.0058}_{-0.0054}$	$0.9591^{+0.0062}_{-0.0051}$
$\mid  au$	$0.0525^{+0.0077}_{-0.0079}$	$0.0552^{+0.0073}_{-0.0077}$	$0.0551^{+0.0072}_{-0.0076}$
$f_{ m fs}$	> 0.74	> 0.80	> 0.80
$H_0 [\mathrm{km/s/Mpc}]$	$67.82^{+0.77}_{-0.79}$	$68.24^{+0.6}_{-0.57}$	$68.27^{+0.47}_{-0.41}$
$r_s^{ m drag} \ [{ m Mpc}]$	$147.04_{-0.41}^{+0.53}$	$147.02^{+0.27}_{-0.27}$	$147.03^{+0.24}_{-0.24}$
$\sigma_8$	$0.8168^{+0.0078}_{-0.0073}$	$0.8173^{+0.0072}_{-0.0073}$	$0.8171^{+0.0078}_{-0.0068}$
$\chi^2_{ m tot}$	1189.06	2774.07	2780.92

Table 1. Results for a model with  $N_{\rm tot} = 3.046$  with varying  $f_{\rm fs}$  fraction of free-streaming radiation species. We present the marginalized mean  $\pm 1\,\sigma$  error for all the parameters, with the exception of  $f_{\rm fs}$  for which we show the 95% lower limit. The  $\chi^2_{\rm tot}$  values correspond to best-fit point found using numerical minimization.

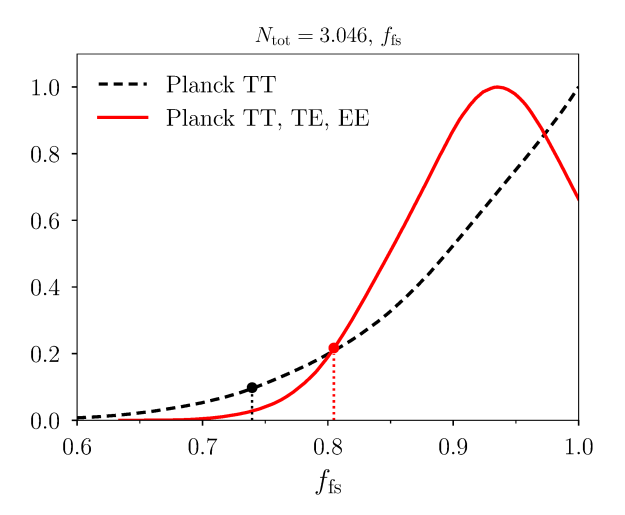


Figure 1. Marginalized posteriors of the fraction of energy in free-streaming radiation,  $f_{\rm fs}$ , in the model with fixed  $N_{\rm tot}=3.046$  using only Planck data. The dashed black and solid red lines correspond to the results using *Planck* TT, and TT, TE, EE data sets, respectively. The solid points denote the 95.4% CL lower limit on  $f_{\rm fs}$  for each data set taken from table 1.

the full polarization data. In each case there is no preference for  $f_{\rm fs} < 1$  at greater than  $1\sigma$ . Such a preference emerges if one combines the CMB data with the local  $H_0$  measurement; however, because this model does not have any additional energy density and therefore does not address the  $H_0$  tension, the two data sets are discrepant at  $> 2\sigma$  and the small preference for non-zero interacting radiation component is irrelevant.

	$\Lambda \mathrm{CDM}$	$N_{ m eff}$	$N_{\rm eff}=3.046,N_{\rm fld}$	$N_{ m tot},f_{ m fs}$
$100\theta_s$	$1.0419^{+0.0003}_{-0.0003}$	$1.0422^{+0.00054}_{-0.00057}$	$1.042^{+0.00032}_{-0.00032}$	$1.0429^{+0.00062}_{-0.0007}$
$100\Omega_b h^2$	$2.237^{+0.015}_{-0.015}$	$2.223^{+0.024}_{-0.021}$	$2.254^{+0.017}_{-0.021}$	$2.236^{+0.024}_{-0.025}$
$\Omega_c h^2$	$0.1199^{+0.0011}_{-0.0013}$	$0.1176^{+0.0031}_{-0.003}$	$0.1221^{+0.0016}_{-0.0025}$	$0.1187^{+0.003}_{-0.0032}$
$\ln 10^{10} A_s$	$3.043^{+0.014}_{-0.015}$	$3.036^{+0.017}_{-0.018}$	$3.044^{+0.014}_{-0.015}$	$3.026^{+0.019}_{-0.019}$
$n_s$	$0.9649^{+0.0046}_{-0.0038}$	$0.9585^{+0.0091}_{-0.0089}$	$0.9673^{+0.0042}_{-0.0048}$	$0.9563^{+0.0084}_{-0.0083}$
$\mid  au$	$0.054^{+0.0068}_{-0.0076}$	$0.0534^{+0.0071}_{-0.0079}$	$0.0557^{+0.0073}_{-0.0081}$	$0.0546^{+0.0069}_{-0.0082}$
$N_{ m tot}$	3.046	$2.89^{+0.21}_{-0.2}$	$3.197^{+0.037}_{-0.151}$	$2.96^{+0.2}_{-0.21}$
$f_{ m fs}$	1	1	> 0.89	> 0.81
$H_0 [\mathrm{km/s/Mpc}]$	$67.93^{+0.54}_{-0.55}$	$66.8^{+1.6}_{-1.5}$	$69.14_{-1.26}^{+0.77}$	$67.7^{+1.4}_{-1.7}$
$r_s^{ m drag} \ [{ m Mpc}]$	$147.14_{-0.26}^{+0.27}$	$148.8^{+1.9}_{-2.1}$	$145.6_{-0.6}^{+1.5}$	$147.9^{+2.0}_{-2.0}$
$\sigma_8$	$0.8232^{+0.0057}_{-0.0059}$	$0.816^{+0.01}_{-0.011}$	$0.8264^{+0.0066}_{-0.0069}$	$0.814^{+0.01}_{-0.011}$
$\chi^2_{ m tot}$	2774.75	2772.88	2774.75	2772.79

Table 2. Comparison of extensions of  $\Lambda$ CDM with extra radiation degrees of freedom for the *Planck* TT, TE, EE likelihood. We present the marginalized mean  $\pm 1\,\sigma$  error for all the parameters, with the exception of  $f_{\rm fs}$  for which we show the 95% lower limit. The  $\chi^2_{\rm tot}$  values correspond to best-fit point found using numerical minimization.

#### 4.2 Models with varying $N_{\text{tot}}$

The results for models with varying  $N_{\rm tot}$  are presented in tables 2 (*Planck* TT, TE, EE), 3 (*Planck* TT, TE, EE + BAO) and 4 (*Planck* TT, TE, EE + BAO +  $H_0$ ), with  $\Lambda$ CDM and an  $N_{\rm eff}$  model included for completeness (see appendix A for results using only the TT likelihood). We highlight some of the interesting features below.

- CMB data requires the presence of free streaming species with at least  $f_{\rm fs} > 0.8 0.9$  depending on the model and data set
- CMB and BAO data do not show preference for additional interacting or free-streaming species
- When combined with the local measurement of  $H_0$ , a strong preference for additional radiation emerges
- This improvement comes at the price of a worse fit to the high- $\ell$  multipoles in part due to the larger effect of diffusion damping
- Non-free-streaming allows for a slightly larger radiation component resulting in a mild improvement in fitting  $H_0$  compared to models with only free-streaming radiation.

We elaborate on these observations below.

Extra radiation and  $H_0$ . An increase in the total amount of radiation, interacting or free-streaming, leads to an increase in  $H_0$ . This is easily understood from the fact that the extra radiation decreases the size of the sound horizon, as discussed in section 3, which requires a decrease in the angular distance  $D_A$  in order to keep the position of the peaks

	$\Lambda \mathrm{CDM}$	$N_{ m eff}$	$N_{\rm eff} = 3.046,  N_{\rm fld}$	$N_{ m tot},f_{ m fs}$
$100\theta_s$	$1.0419^{+0.00027}_{-0.00031}$	$1.0422^{+0.00053}_{-0.0005}$	$1.042^{+0.0003}_{-0.0003}$	$1.0429^{+0.00063}_{-0.00075}$
$100\Omega_b h^2$	$2.239^{+0.014}_{-0.013}$	$2.232^{+0.017}_{-0.02}$	$2.252^{+0.015}_{-0.017}$	$2.24^{+0.019}_{-0.021}$
$\Omega_c h^2$	$0.11964^{+0.0009}_{-0.00092}$	$0.118^{+0.0027}_{-0.0031}$	$0.122^{+0.0014}_{-0.0026}$	$0.1191^{+0.0031}_{-0.0032}$
$\ln 10^{10} A_s$	$3.044^{+0.012}_{-0.016}$	$3.039^{+0.016}_{-0.015}$	$3.043^{+0.013}_{-0.014}$	$3.027^{+0.018}_{-0.018}$
$n_s$	$0.9655^{+0.0037}_{-0.0038}$	$0.9621^{+0.007}_{-0.0072}$	$0.9671^{+0.0039}_{-0.0042}$	$0.9573^{+0.0081}_{-0.0077}$
$\mid  au$	$0.0545^{+0.0065}_{-0.0076}$	$0.0543^{+0.0068}_{-0.0075}$	$0.0553^{+0.0068}_{-0.0072}$	$0.0549^{+0.0068}_{-0.0077}$
$N_{ m tot}$	3.046	$2.94^{+0.16}_{-0.19}$	$3.192^{+0.032}_{-0.146}$	$2.99^{+0.18}_{-0.19}$
$f_{ m fs}$	1	1	> 0.89	> 0.80
$H_0 [\mathrm{km/s/Mpc}]$	$68.05^{+0.44}_{-0.41}$	$67.4^{+1.1}_{-1.2}$	$69.09_{-1.08}^{+0.62}$	$67.9^{+1.2}_{-1.3}$
$r_s^{\text{drag}} [\text{Mpc}]$	$147.18^{+0.23}_{-0.21}$	$148.3^{+1.8}_{-1.7}$	$145.7^{+1.5}_{-0.6}$	$147.6^{+1.9}_{-1.9}$
$\sigma_8$	$0.8227^{+0.0057}_{-0.0062}$	$0.8178^{+0.0094}_{-0.0102}$	$0.8261^{+0.0063}_{-0.0066}$	$0.815^{+0.01}_{-0.01}$
$\chi^2_{ m tot}$	2781.06	2780.95	2781.04	2780.95

Table 3. Comparison of extensions of  $\Lambda$ CDM with extra radiation degrees of freedom for *Planck* TT, TE, EE + BAO likelihood. We present the marginalized mean  $\pm 1\,\sigma$  error for all the parameters, with the exception of  $f_{\rm fs}$  for which we show the 95% lower limit. The  $\chi^2_{\rm tot}$  values correspond to best-fit point found using numerical minimization.

	$\Lambda \mathrm{CDM}$	$N_{ m eff}$	$N_{\rm eff} = 3.046, N_{\rm fld}$	$N_{ m tot},f_{ m fs}$
$100\theta_s$	$1.042^{+0.00029}_{-0.00028}$	$1.0414^{+0.00043}_{-0.00049}$	$1.0423^{+0.0003}_{-0.00032}$	$1.0427^{+0.00074}_{-0.00088}$
$100\Omega_b h^2$	$2.249^{+0.013}_{-0.015}$	$2.265^{+0.017}_{-0.016}$	$2.275^{+0.016}_{-0.018}$	$2.275^{+0.018}_{-0.017}$
$\Omega_c h^2$	$0.11861^{+0.00093}_{-0.00092}$	$0.1229^{+0.0026}_{-0.0026}$	$0.1248^{+0.0026}_{-0.0029}$	$0.1244^{+0.0029}_{-0.0029}$
$\ln 10^{10} A_s$	$3.049^{+0.014}_{-0.015}$	$3.058^{+0.015}_{-0.016}$	$3.043^{+0.014}_{-0.016}$	$3.036^{+0.021}_{-0.019}$
$n_s$	$0.9681^{+0.0035}_{-0.004}$	$0.9761^{+0.0061}_{-0.0057}$	$0.9704^{+0.004}_{-0.0038}$	$0.9669^{+0.0082}_{-0.0075}$
$\tau$	$0.0576^{+0.007}_{-0.0078}$	$0.0575^{+0.007}_{-0.0076}$	$0.0574^{+0.0066}_{-0.0082}$	$0.0575^{+0.007}_{-0.0074}$
$N_{ m tot}$	3.046	$3.3^{+0.15}_{-0.15}$	$3.38^{+0.13}_{-0.15}$	$3.35^{+0.16}_{-0.15}$
$f_{ m fs}$	1	1	$0.901^{+0.039}_{-0.036}$	$0.87^{+0.08}_{-0.06}$
$H_0 [\mathrm{km/s/Mpc}]$	$68.55^{+0.46}_{-0.41}$	$70.0^{+0.93}_{-0.9}$	$70.64^{+0.93}_{-1.0}$	$70.5^{+1.0}_{-1.0}$
$r_s^{\rm drag} \ [{ m Mpc}]$	$147.34_{-0.23}^{+0.22}$	$144.8^{+1.4}_{-1.5}$	$143.9_{-1.3}^{+1.5}$	$144.1_{-1.6}^{+1.5}$
$\sigma_8$	$0.8216^{+0.0061}_{-0.0062}$	$0.8335^{+0.0089}_{-0.0093}$	$0.8299^{+0.0068}_{-0.0078}$	$0.826^{+0.011}_{-0.01}$
$\chi^2_{ m tot}$	2797.46	2795.16	2793.65	2793.44

Table 4. Comparison of extensions of  $\Lambda$ CDM with extra radiation degrees of freedom for the *Planck* TT, TE, EE + BAO +  $H_0$  likelihood. We present the marginalized mean  $\pm 1\,\sigma$  error for all the parameters. The  $\chi^2_{\rm tot}$  values correspond to best-fit point found using numerical minimization.

fixed. This decrease in  $D_A$  is largely driven by an increase in  $H_0$ . The correlation between  $N_{\text{tot}}$  and  $H_0$  can be readily seen in figure 2 for all models where the radiation density is allowed to vary.

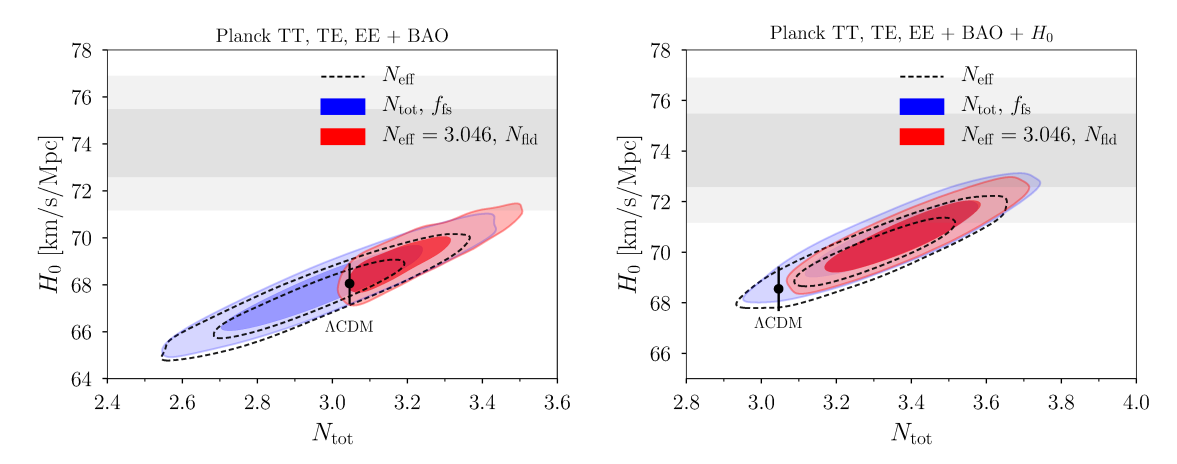


Figure 2. Marginalized posterior of the total radiation degrees of freedom  $N_{\rm tot}$  and the present value of the Hubble rate,  $H_0$ , in different models. In the left panel we combine Planck and BAO data, while in the right we add the distance ladder measurement of  $H_0$  [16]. In both panels the gray horizontal band represents this measurement and the black dot is the  $\Lambda$ CDM value with  $2\sigma$  uncertainties. The darker inner (lighter outer) regions correspond to 68% (95%) confidence regions.

Interacting versus free-streaming radiation. The effect of the phase shift associated with free-streaming species can be directly seen in figure 3. From it one can easily see that in the  $N_{\text{eff}}$  model an increase in the radiation density is anti-correlated with the angular size of the sound horizon. This is expected from the fact that the supersonic propagation of free-streaming radiation shifts the acoustic peaks of the CMB to larger scales. In order to maintain the location of the peak in the power spectrum fixed this requires a decrease in the physical size of the sound horizon angular scale  $\theta_s = r_s/D_A$ , as can be seen from eq. (3.11). The effect of increasing the energy density in interacting radiation on the other hand decreases the phase shift associated with the neutrinos and thus requires an increase in the angular sound horizon scale.

Implications for the Hubble and  $\sigma_8$  tensions. The fraction of interacting radiation allowed by the data is not significantly increased by letting  $N_{
m tot}$  vary as seen in figures 4 and 5. The only exception is when the likelihood for the local  $H_0$  measurements is included in the scan, which brings the allowed range of  $N_{\rm tot}$  to slightly larger values and leads to a mild preference for a non-zero fraction of interacting radiation. This can be partially explained by recalling that the increase in  $N_{\text{tot}}$  required to accommodate a larger  $H_0$  leads to an increase in the ratio between the photon diffusion length and the sound horizon scale. In addition, the presence of free-streaming species decreases the gravitational potential at horizon crossing, and therefore leads to a smaller radiation driving effect for modes that enter the horizon before matter radiation equality. Both of these effects decrease the temperature power spectrum at larger  $\ell$ . Allowing part of the radiation to be interacting increases the size of the gravitational potential at horizon crossing (see eq. (3.7)) in comparison to models with only  $N_{\rm eff}$ , and therefore leads to less suppression of power at high  $\ell$ . This effect enables the data to tolerate slightly larger values of  $N_{\text{tot}}$  as shown in figure 4. This, in turn, leads to a larger overlap of the Planck+BAO  $H_0$  posterior with the local measurement compared to free-streaming radiation, which is illustrated in figure 2. This improvement can be quantified in terms of Gaussian standard deviations by using the (generally non-Gaussian) posterior  $H_0$ distribution to define an effective  $\chi^2$  for the Planck+BAO results. We find that in models

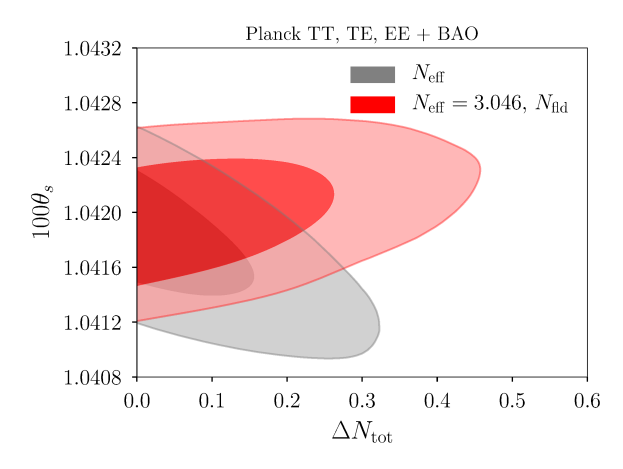


Figure 3. Marginalized posterior of the additional radiation degrees of freedom (either  $\Delta N_{\rm tot} = N_{\rm eff} - 3.046$ , or  $\Delta N_{\rm tot} = N_{\rm fld}$  with  $N_{\rm eff} = 3.046$ ) and the angular scale of the sound horizon  $\theta_s$  as derived from the Planck + BAO data sets. Free-streaming ( $N_{\rm eff}$ ) and non-free-streaming ( $N_{\rm fld}$ ) radiation exhibit different correlation with  $\theta_s$  due to their opposite effects on the phase shift of acoustic peaks in the CMB. Supersonic propagation of free-streaming radiation perturbations shifts acoustic peaks to larger angular scales; in order to keep the physical peak locations the same  $\theta_s$  must be decreased. Conversely, non-free-streaming radiation reduces this phaseshift, requiring  $\theta_s$  to increase to keep peak location the same. The darker inner (lighter outer) regions correspond to 68% (95%) confidence regions.

with varying  $N_{\rm tot}$  and  $f_{\rm fs}$  the  $\sim 4.4\sigma~H_0$  tension (in  $\Lambda{\rm CDM}$  with massive neutrinos) is reduced to  $3.3\sigma$ ; this should compared to the  $3.7\sigma$  tension in the  $N_{\rm eff}$ -only model.

The reduced suppression of power at high- $\ell$  also explains why models with interacting radiation lead to smaller values for  $n_s$  compared to free-streaming only models as can be seen in table 4. The smaller value for  $n_s$  leads to a smaller  $\sigma_8$  for models with interacting radiation in comparison to models with only free-streaming species. However, as shown in figure 6, when looking at  $S_8 = \sigma_8 \sqrt{\Omega_m/0.3}$  (a quantity more directly related to measurements), both models are within the  $2\sigma$  allowed region of low-z measurement of ref. [38],  $S_8 = 0.801^{+0.028}_{-0.026}$ .

In table 5 we break down the  $\chi^2$  for the best fit points to the *Planck* TT, TE, EE + BAO +  $H_0$  likelihood for each model by the different likelihoods used. We find that for all of the models the improvement in  $\chi^2$  is driven almost exclusively by the improved fit to the  $H_0$  likelihood. In particular all models provide a worse fit to the CMB power spectrum, except at low- $\ell$  ( $\ell \leq 29$ ), where they improve the temperature power spectrum and for the models with  $N_{\rm fld}$  there is also improvement for low- $\ell$  polarization.

Variation of primordial helium fraction  $Y_p$ . It is well known that there is a partial degeneracy between  $N_{\text{tot}}$  and  $Y_p$  due to their effects on the diffusion damping scale (see the discussion around eq. (3.9) and, e.g., ref. [12] for a clear explanation). In order to see the maximum effect of  $Y_p$  in reducing the Hubble tension we considered models with freely varying  $N_{\text{tot}}$  and  $Y_p$  (i.e.,  $Y_p$  is not calculated from BBN). The results for those runs are shown in table 6. One sees that the extra freedom to adjust  $Y_p$  significantly increases the allowed range for  $N_{\text{tot}}$  and consequently also for  $H_0$ . These results are relevant to cosmological scenarios where  $Y_p$  can vary independently of  $N_{\text{tot}}$ , which can occur in some of the models described in section 2. However, aside from the BBN consistency requirement, there are also direct measurements of the primordial <sup>4</sup>He abundance which place constraints on  $Y_p$  that only depend on late Universe considerations. We have explored the effects of

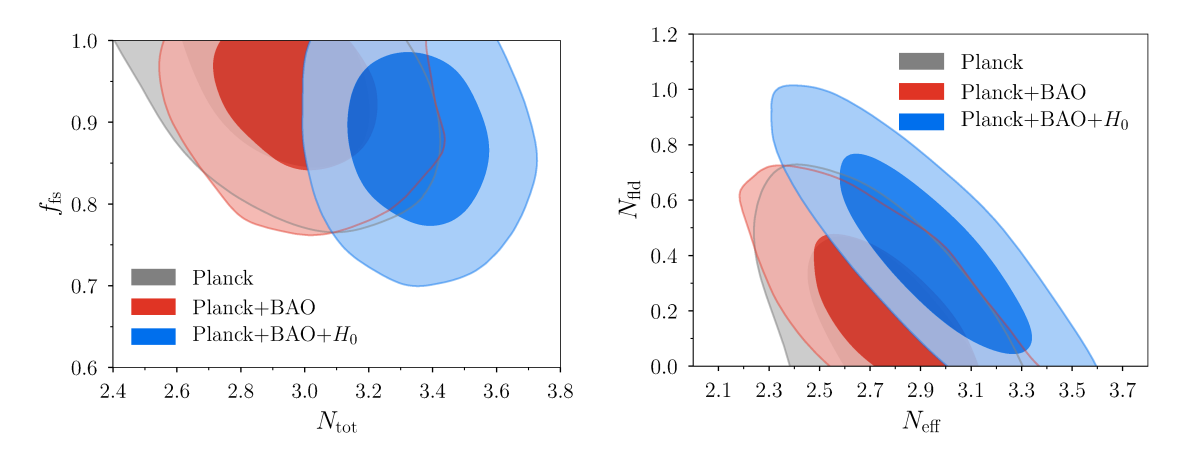


Figure 4. Marginalized posterior for the model with free-streaming and non-free-streaming species for different combinations of cosmological data. In the left panel the posterior is shown as a function of the total radiation degrees of freedom  $N_{\rm tot}$  and their free-streaming fraction  $f_{\rm fs}$ , while the right panel instead uses the number of free-streaming and non-free-streaming relativistic degrees of freedom,  $N_{\rm eff}$  and  $N_{\rm fld}$ , respectively. In all cases, the darker inner (lighter outer) regions correspond to 68% (95%) confidence regions.

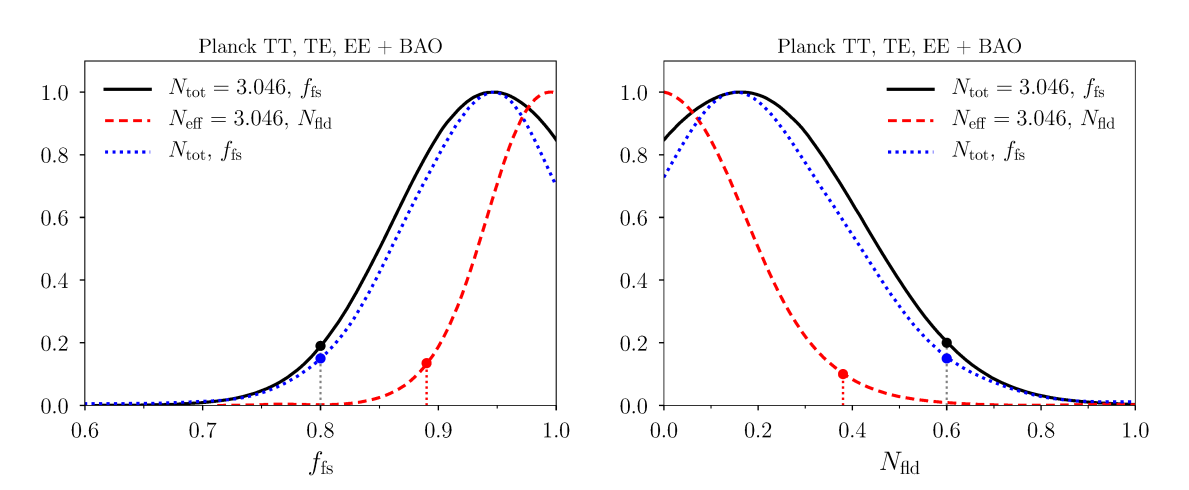


Figure 5. Marginalized posteriors of the fraction of energy in free-streaming radiation  $f_{\rm fs}$  (left panel) and the number of non-free-streaming degrees of freedom  $N_{\rm fld}$  (right panel) in models with fixed and varying  $N_{\rm tot}$  (solid, and dashed or dotted lines, respectively) for the Planck TT, TE, EE + BAO data set. The solid dots denote the 95.4% CL lower (upper) limit on  $f_{\rm fs}$  ( $N_{\rm fld}$ ) in the left (right) panel. These limits happen to coincide for the ( $N_{\rm tot} = 3.046, f_{\rm fs}$ ) and ( $N_{\rm tot}, f_{\rm fs}$ ) models — see tables 1 and 3.

including such measurements in cosmological fits as an additional Gaussian prior with  $Y_p = 0.2449 \pm 0.0040$  [83]. We compare the results for runs including a  $Y_p$  prior to those without in figures 7 and 8. One can directly see from the figures that the inclusion of the local measurements as a prior leads to very similar results to using BBN to determine  $Y_p$ , and therefore does not significantly improve the fit to local  $H_0$  measurements.

#### 4.3 Particle physics interpretation

In this section we interpret our results in terms of the illustrative models described in section 2.

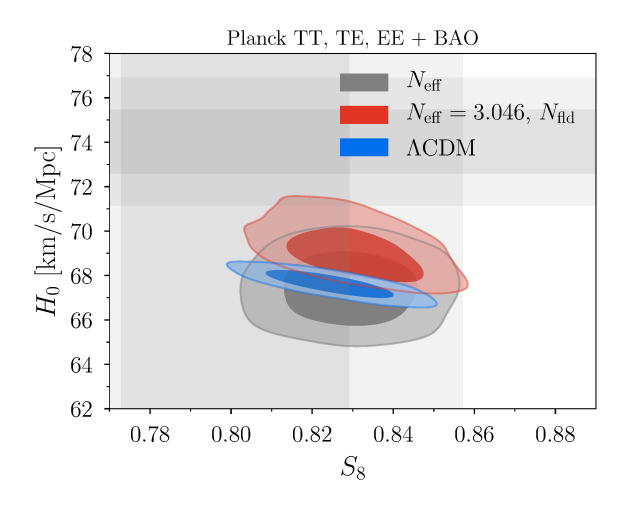


Figure 6. Marginalized posteriors of  $H_0$  and  $S_8 = \sigma_8 \sqrt{\Omega_m/0.3}$  in different models (colored regions) for *Planck* TT, TE, EE + BAO data set and the corresponding direct late-time measurements (gray bands) from refs. [16] and [38]. The darker inner and lighter outer contours correspond to 68% and 95% confidence regions, respectively.

Data Set	$N_{ m eff}$	$N_{\rm eff} = 3.046, \ N_{\rm fld}$	$N_{ m tot},\ f_{ m fs}$
TTTEEE	+2.68	+6.24	+6.24
low-ℓ TT	-0.63	-0.56	-0.56
low-ℓ EE	+0.09	-1.06	-0.29
lensing	+0.17	+0.8	+0.39
BAO	+0.39	+0.73	+1.04
$H_0$	-4.99	-9.93	-10.81
total	-2.3	-3.81	-4.02

**Table 5**. Best fit  $\Delta \chi^2 = \chi^2 - \chi^2_{\Lambda \text{CDM}}$  for models with extra radiation species. In each case the best fit points correspond to the full Planck + BAO +  $H_0$  data set combination of likelihoods. Low- $\ell$  refers to the  $\ell \leq 29$  Planck likelihoods.

Non-Abelian dark radiation. First, we translate the constraints on  $N_{\text{fld}}$  into an upper bound on the number of dark gluons  $N_d$  and the ratio of DR to SM temperature using eq. (2.7)

$$N_d \left(\frac{T_d}{T_\gamma}\right)^4 \le \begin{cases} 0.087 & 95\% \text{ C.L. } (N_{\text{eff}} = 3.046, N_{\text{fld}}) \\ 0.14 & 95\% \text{ C.L. } (N_{\text{eff}}, N_{\text{fld}}), \end{cases}$$
 (4.1)

where we used the Planck+BAO results from table 3 and figure 5. We see that allowing both  $N_{\rm eff}$  and  $N_{\rm fld}$  to vary leads to somewhat weaker constraints. Note that this result does not assume that the DR and SM sectors were ever in thermal equilibrium. However, if there exists a coupling between the non-Abelian dark sector, it must necessarily be through a higher dimensional operator. In this case it is natural for the SM and DS to be in equilibrium at early times but decoupled at late times, leading to a prediction for the temperature ratio  $T_d/T_{\gamma}$  given in eq. (2.6). This prediction only depends on the SM-DR decoupling

	TT, TE, EE	TT, TE, EE + BAO	$TT, TE, EE + BAO + H_0$
$100\theta_s$	$1.0428^{+0.0011}_{-0.001}$	$1.0428^{+0.00093}_{-0.00102}$	$1.0417^{+0.00085}_{-0.00106}$
$100\Omega_b h^2$	$2.24^{+0.023}_{-0.026}$	$2.241^{+0.019}_{-0.021}$	$2.26^{+0.019}_{-0.019}$
$\Omega_c h^2$	$0.1201^{+0.0049}_{-0.0062}$	$0.1198^{+0.0043}_{-0.0052}$	$0.1295^{+0.0044}_{-0.0046}$
$\ln 10^{10} A_s$	$3.026^{+0.019}_{-0.02}$	$3.027^{+0.019}_{-0.017}$	$3.033^{+0.02}_{-0.019}$
$n_s$	$0.9565^{+0.0089}_{-0.0086}$	$0.9572^{+0.0084}_{-0.0075}$	$0.9613^{+0.0091}_{-0.0079}$
$\tau$	$0.0547^{+0.0074}_{-0.0081}$	$0.0551^{+0.0067}_{-0.0074}$	$0.0551^{+0.0072}_{-0.0079}$
$N_{ m tot}$	$3.05^{+0.33}_{-0.41}$	$3.04^{+0.26}_{-0.33}$	$3.66^{+0.26}_{-0.26}$
$f_{ m fs}$	> 0.78	> 0.79	$0.867^{+0.078}_{-0.059}$
$Y_p$	$0.241^{+0.022}_{-0.019}$	$0.241^{+0.02}_{-0.018}$	$0.217^{+0.019}_{-0.019}$
$H_0 [\mathrm{km/s/Mpc}]$	$68.2^{+2.0}_{-2.7}$	$68.2_{-1.8}^{+1.5}$	$71.6^{+1.3}_{-1.2}$
$r_s^{\text{drag}}$ [Mpc]	$147.1^{+3.6}_{-3.2}$	$147.2^{+2.8}_{-2.7}$	$141.7^{+2.2}_{-2.2}$
$\sigma_8$	$0.815^{+0.011}_{-0.012}$	$0.815^{+0.011}_{-0.011}$	$0.829^{+0.011}_{-0.01}$
$\chi^2_{ m tot}$	2774.55	2781.46	2788.85

**Table 6.** Results for a model with  $N_{\rm tot}$ ,  $f_{\rm fs}$  and varying  $Y_p$  (disregarding its direct measurement). We present the marginalized mean  $\pm 1\,\sigma$  error for all the parameters, with the exception of  $f_{\rm fs}$  for which we show the 95% lower limit.

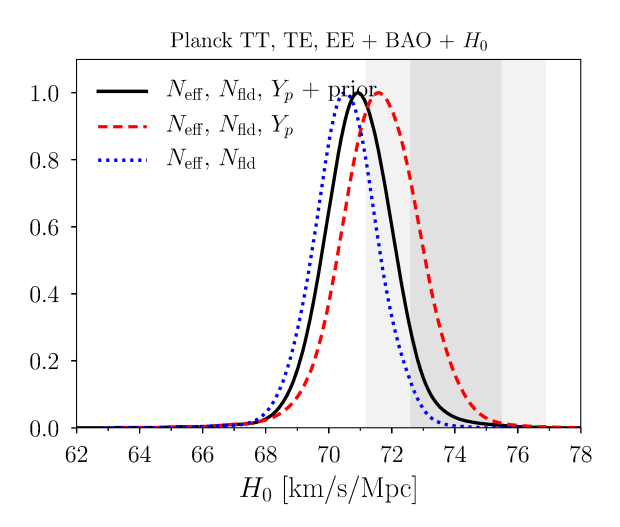


Figure 7. Marginalized posteriors of  $H_0$  for the  $(N_{\rm eff}, N_{\rm fld})$  model with  $Y_p$  fixed by BBN (blue dotted), or allowed to vary disregarding direct measurements (red dashed) and including direct measurements (black solid). The gray band shows the local  $H_0$  measurement [16], with darker inner and lighter outer contours corresponding to  $1\sigma$  and  $2\sigma$  confidence regions, respectively.

temperature  $T_f$ , and the assumption that there was no non-SM entropy injection between  $T_f$  and today. In figure 9 we show the constraints implied by eq. (4.1) and the early-time equilibrium hypothesis. In the left panel the prediction of eq. (2.7) for two gauge groups is shown as a function of  $T_f$  illustrating the constraining power of cosmological data. The strongest cosmological constraints, for example, rule out DR from an SU(3) sector that was in equilibrium with the SM at any temperature. In the right panel of figure 9 we show the

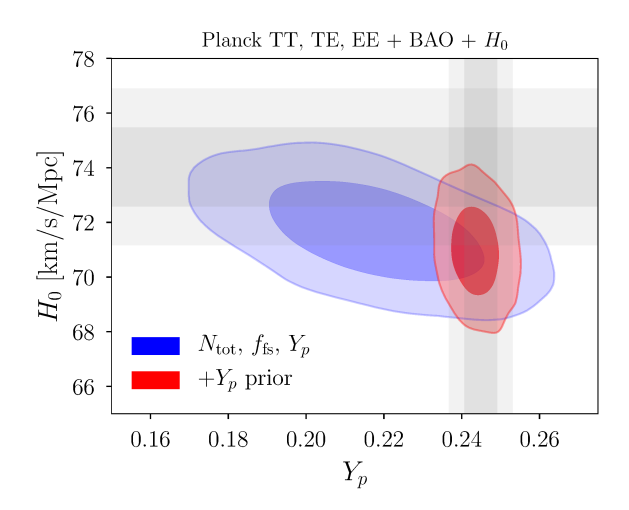


Figure 8. Marginalized posteriors of  $H_0$  and  $Y_p$  for the  $(N_{\rm eff}, N_{\rm fld})$  model with  $Y_p$  allowed to vary disregarding direct measurements (blue) and including direct measurements as a prior (red). The gray bands show the direct late-time measurements of  $H_0$  [16] (horizontal band) and  $Y_p$  [83] (vertical band), with darker inner and lighter outer contours corresponding to  $1\sigma$  and  $2\sigma$  confidence regions, respectively.

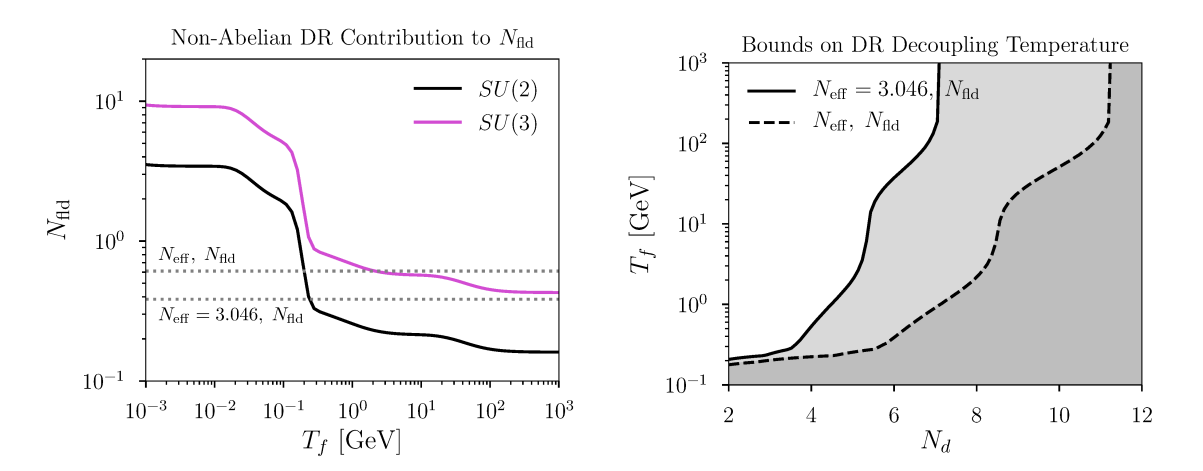


Figure 9. Constraints on non-Abelian dark radiation that decoupled from the SM at temperature  $T_f$ . In the left panel we show the predictions for  $N_{\rm fld}$  as a function of  $T_f$  for DR from an SU(2) (SU(3)) dark sector as the lower (upper) solid line. Upper bounds on  $N_{\rm fld}$  from ( $N_{\rm eff}$ ,  $N_{\rm fld}$ ) and ( $N_{\rm eff} = 3.046, N_{\rm fld}$ ) scans using Planck+BAO data are shown as dotted gray lines. In the right panel we translate these constraints into bounds on  $T_f$  as a function of the number of dark gluons  $N_d$  (e.g.,  $N_d = 3$  in SU(2)). Gray shaded region is excluded at 95% C.L.

lower bound on  $T_f$  as a function of the number of dark gluons  $N_d$ . The strongest Planck and BAO constraints therefore exclude the possibility of a non-free-streaming dark sector with  $N_d > 7$  being in thermal equilibrium with the SM at any temperature (again, assuming no non-standard entropy injections after  $T_f$ ).

Late equilibration of a dark sector. Our results can be used to constrain several limits of the late equilibration scenario described in section 2.2. The most straightforward application is the case when a neutrino-coupled mediator  $\phi$  equilibrates with one or more neutrinos well

before modes relevant for the CMB enter the horizon; this occurs if

$$\sqrt{\lambda_{\nu}} m_{\phi} \gtrsim 6 \times 10^{-6} \text{ eV},$$
 (4.2)

where we used eq. (2.11), taking  $T_{\phi}^{\rm nfs} \gtrsim 20(4/11)^{1/3}$  eV (roughly corresponding to the time when modes with  $k \sim 0.2/{\rm Mpc}$  enter the horizon). The equilibrium must persist until well after matter-radiation equality, requiring  $m_{\phi} \ll {\rm eV}^{.6}$  These conditions ensure that  $N_{\rm tot} \approx 3$  and that the  $\phi - \nu$  bath behaves as a relativistic fluid throughout the CMB era. This scenario then directly maps onto the  $(N_{\rm tot} = 3.046, f_{\rm fs})$  scan, with the naive expectation that at least one neutrino species is not free-streaming. In figure 1 and table 1 we found that the free-streaming fraction has to be larger than 0.8 at 95% C.L. for the CMB+BAO dataset, robustly excluding this part of the late equilibration parameter space.

The second possibility highlighted in section 2.2 was that  $\phi$  is a portal to a larger dark sector (with a total number N' degrees of freedom), so late equilibration also populates these additional states. If some number  $N_h$  of these particles are "heavy", i.e. they become non-relativistic before the CMB era, they will heat the remaining interacting particles compared to the SM, which increases  $N_{\rm tot}$ . There are two interesting limits of this scenario. First, we assume that the remaining DS states stay in equilibrium with neutrinos throughout the CMB era. Then, the only contributions to the free-streaming fraction  $f_{\rm fs}$  come from those neutrino mass eigenstates that do not interact with the DS:

$$f_{\rm fs} \approx \frac{3 - N_{\nu}}{N_{\rm tot}},$$
 (4.3)

where  $N_{\nu}$  is the number of interacting neutrinos and  $N_{\rm tot}$  is given by eq. (2.16). This scenario is generalization of the one described in the previous paragraph, which allows for  $N_{\rm tot} > 3$ . The prediction this model is shown in figure 10 for  $N_{\nu} = 1$ , varying N' and different choices of  $N_h$ . Note that since the numerator of eq. (4.3) only depends on  $N_{\nu}$ , all choices of  $N_h$  collapse onto the same contour. It is also clear from this equation that we expect  $f_{\rm fs} < 2/3$  for this scenario, which is robustly excluded by cosmological data.

The second interesting limit corresponds to the case where the  $N_h$  heavy states include the mediator  $\phi$ . When these particles become non-relativistic, they heat both the interacting neutrino and the light DS states; however, after this point the neutrinos and the DS are decoupled. In this case, all neutrino eigenstates contribute to  $f_{\rm fs}$ , but  $N_{\nu}$  of them have a distinct temperature; we find that

$$f_{\rm fs} \approx \frac{1}{N_{\rm tot}} \left[ 3 - N_{\nu} + N_{\nu} \left( \frac{N_{\nu}}{N_{\nu} + N'} \right) \left( \frac{N_{\nu} + N'}{N_{\nu} + N' - N_h} \right)^{4/3} \right],$$
 (4.4)

where  $N_{\rm tot}$  is given in eq. (2.16). The predictions for this scenario are shown by blue dashed lines in figure 10 for  $N_{\nu}=1$ . In contrast to the previous case, the temperature of the now-decoupled  $N_{\nu}$  eigenstates depends on  $N_h$ , which ensures that different choices of this quantity give different predictions in the  $N_{\rm tot}-f_{\rm fs}$  plane. In all cases, however, for  $N'\gg N_{\nu}$ ,  $N_h$  the contribution of the  $N_{\nu}$  neutrinos to  $f_{\rm fs}$  is diluted as the energy is shared amongst many DS states, and  $f_{\rm fs}$  approaches 2/3 (i.e. only the non-interacting  $3-N_{\nu}$  neutrinos contribute to

 $<sup>^6</sup>$ If  $m_{\phi} \gg {\rm eV}$ , the mediator goes non-relativistic and heats the neutrinos relative to photons, increasing  $N_{\rm eff}$  without changing neutrino free-streaming during the CMB epoch. Bounds on  $\Delta N_{\rm eff}$  can be applied in this regime. If the non-relativistic transition occurs during the CMB era, a different analysis is required since the equation of state of the  $\phi - \nu$  fluid and phase-space distributions have non-trivial evolution.

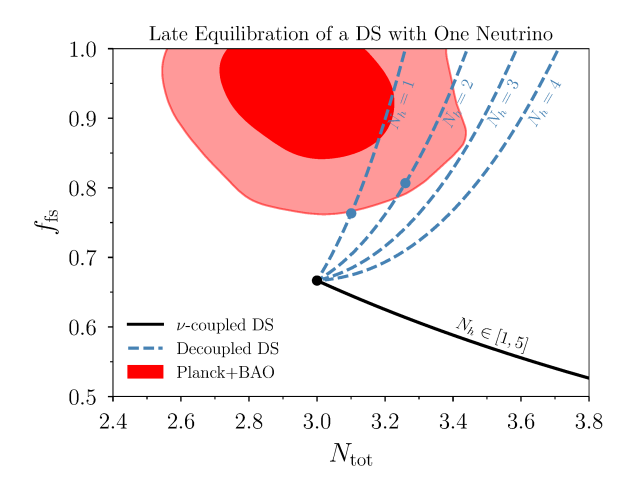


Figure 10. Predictions of models with late equilibration of a dark sector (DS) that couples to a single neutrino mass eigenstate. The black line shows the case where the DS remains coupled to that neutrino throughout the CMB epoch, so that the only free-streaming species are the remaining two neutrinos. This contour is obtained by varying the total number of DS states N' and the number of "heavy" states  $N_h$  that become non-relativistic after equilibration but before the CMB epoch. Larger  $N_h$  results in a higher density of non-free-streaming states, thereby lowering  $f_{\rm fs}$ . The dashed blue lines show the predictions of an alternative scenario where after equilibration,  $N_h$  DS states become non-relativistic, including the mediator responsible for  $\nu$ -DS interaction, thereby decoupling the two sectors once again. This heats both the DS states and the single neutrino eigenstate; now, however, all neutrinos contribute to the free-streaming fraction, including the one that used to interact with the DS. The dots on the  $N_h = 1$  and 2 lines correspond to N' = 3, with larger N' falling below the dots. The Planck+BAO posterior distribution (see figure 4) is shown in red with the darker inner (lighter outer) regions corresponding to 68% (95%) confidence regions.

the free-streaming fraction as before). In the other limit  $N' \sim N_h f_{\rm fs}$  approaches 1 — the only remaining light relics are neutrinos with a slightly higher total energy density, resulting in  $N_{\rm tot} > 3$ . We see in figure 10 that cosmological data is able to distinguish between these different scenarios and place severe constraints on models with N' > 3 or  $N_h > 2$ . We emphasize that these constraints apply as long as the equilibration and non-relativistic transitions occur outside of the CMB era. If this is not the case, then the various fluids have time-dependent equations of state and free-streaming behavior which is not captured by the simple cosmological model described in section 3.

#### 5 Conclusion

In this paper we have studied the status of cosmological models with extra radiation after Planck's final data release, allowing part of that radiation to be non-free-streaming. We also considered combinations of Planck's results with BAO and direct measurements of  $H_0$ .

When restricting the total radiation to be equal to that predicted by  $\Lambda$ CDM,  $N_{\text{tot}} = 3.046$ , we find that Planck data alone requires the fraction of free-streaming radiation to be larger than 80%. This shows that none of the neutrino flavors can have non-negligible interactions during the CMB epoch.

If the total amount of radiation is allowed to vary, we find that models which have an interacting component allow for slightly larger values of  $N_{\text{tot}}$ , and therefore larger values for  $H_0$ . This reduces the tension between local measurements of  $H_0$  and the CMB. Both the

model with only extra interacting components and the model in which both free-streaming and non-free-streaming components are allowed to vary improve the total  $\chi^2$  compared to the  $N_{\rm eff}$  case. However, if one takes into consideration the number of extra degrees of freedom in each model, ( $N_{\rm eff}=3.046,N_{\rm fld}$ ) is the one most favored by data.

Interacting radiation models also lead to slightly lower values for  $n_s$  when compared to free-streaming radiation models with the same total amount of radiation. This leads to smaller values for  $\sigma_8$  which results in less tension between solutions to the  $H_0$  tension and matter power spectrum measurements.

We also showed that the cosmological data is able to distinguish and constrain interesting particle physics models of interacting dark radiation, including non-Abelian dark sectors and late equilibration of neutrino-coupled particles. In these models we focused on the parameter space where self-interactions within the fluid component are always in equilibrium. In many interesting scenarios these reactions fall out of or enter equilibrium — see, e.g., refs. [26, 27]. If this occurs during the CMB era, it can leave a characteristic imprint on the power spectrum, possibly allowing further improvements to the fit of all cosmological data. These decoupling (or re-coupling) effects have been studied within the context of specific models relating to neutrino self-interactions. It would be interesting to investigate the impact of the final Planck data release on these and more general frameworks such as that of ref. [64].

#### Acknowledgments

We thank Francis-Yan Cyr-Racine, Deanna Hooper, Vivian Poulin, David E. Kaplan, Celeste Keith, Jose Bernal, Graeme Addison and Marilena LoVerde for useful conversations. We thank Yuhsin Tsai for useful discussions and comments on the draft. This manuscript has been authored by Fermi Research Alliance, LLC under Contract No. DE-AC02-07CH11359 with the U.S. Department of Energy, Office of Science, Office of High Energy Physics. The research of GMT was supported in part by the NSF under Grant No. PHY-1914480, PHY-1914731 and by the Maryland Center for Fundamental Physics (MCFP). We thank the Galileo Galilei Institute for Theoretical Physics for the hospitality and the INFN for partial support during the completion of this work. GMT acknowledges the KITP where part of this work was completed, supported in part by the National Science Foundation under Grant No. NSF PHY-1748958. We used GetDist [84] to generate the figures in this work.

#### A Planck TT results

The constraints using only the *Planck* TT likelihood for the models with varying  $N_{\text{tot}}$  are given in table 7.

	$\Lambda \mathrm{CDM}$	$N_{ m eff}$	$N_{\rm eff} = 3.046, N_{\rm fld}$	$N_{ m tot},f_{ m fs}$
$100\theta_s$	$1.0418^{+0.00044}_{-0.00043}$	$1.042^{+0.00068}_{-0.00068}$	$1.042^{+0.00045}_{-0.00045}$	$1.0429^{+0.00085}_{-0.00118}$
$100\Omega_b h^2$	$2.214^{+0.022}_{-0.021}$	$2.209^{+0.031}_{-0.032}$	$2.232^{+0.024}_{-0.028}$	$2.219_{-0.031}^{+0.033}$
$\Omega_c h^2$	$0.12^{+0.0016}_{-0.0016}$	$0.1188^{+0.0038}_{-0.0043}$	$0.1223^{+0.0019}_{-0.0028}$	$0.1196^{+0.0039}_{-0.0039}$
$\ln 10^{10} A_s$	$3.039^{+0.014}_{-0.015}$	$3.035^{+0.022}_{-0.02}$	$3.038^{+0.015}_{-0.015}$	$3.019^{+0.027}_{-0.022}$
$n_s$	$0.9636^{+0.0049}_{-0.005}$	$0.96^{+0.012}_{-0.013}$	$0.9659^{+0.0054}_{-0.0049}$	$0.953^{+0.014}_{-0.014}$
$\mid  au$	$0.0522^{+0.0077}_{-0.0076}$	$0.0518^{+0.0083}_{-0.008}$	$0.0532^{+0.0081}_{-0.0084}$	$0.0521^{+0.0079}_{-0.0083}$
$N_{ m tot}$	3.046	$2.96^{+0.27}_{-0.3}$	$3.197^{+0.039}_{-0.151}$	$2.96^{+0.28}_{-0.27}$
$f_{ m fs}$	1	1	> 0.88	> 0.72
$H_0 [\mathrm{km/s/Mpc}]$	$67.69^{+0.73}_{-0.77}$	$67.1^{+2.1}_{-2.3}$	$68.87^{+0.87}_{-1.5}$	$67.2^{+2.1}_{-2.2}$
$r_s^{ m drag} \ [{ m Mpc}]$	$147.37^{+0.41}_{-0.35}$	$148.2^{+2.6}_{-2.8}$	$145.8^{+1.7}_{-0.7}$	$147.9^{+2.4}_{-2.7}$
$\sigma_8$	$0.8222^{+0.0064}_{-0.0063}$	$0.819^{+0.013}_{-0.013}$	$0.8252^{+0.0073}_{-0.0072}$	$0.813^{+0.013}_{-0.013}$
$\chi^2_{ m tot}$	1189.2	1188.93	1189.11	1188.41

Table 7. Comparison of extensions of  $\Lambda$ CDM with extra radiation degrees of freedom for the *Planck* TT likelihood. We present the marginalized mean  $\pm 1\,\sigma$  error for all the parameters, with the exception of  $f_{\rm fs}$  for which we show the 95% lower limit. The  $\chi^2_{\rm tot}$  values correspond to best-fit point found using numerical minimization.

#### B Posterior distributions

Here we present the full combination of 2d posterior distributions for the model with  $N_{\text{fld}}$  only (figure 11) and with  $N_{\text{eff}} + N_{\text{fld}}$  (figure 12) using the Planck TT, TE, EE + BAO likelihood combination, and demonstrate the impact of an additional prior on  $H_0$  from the local measurement of ref. [16].

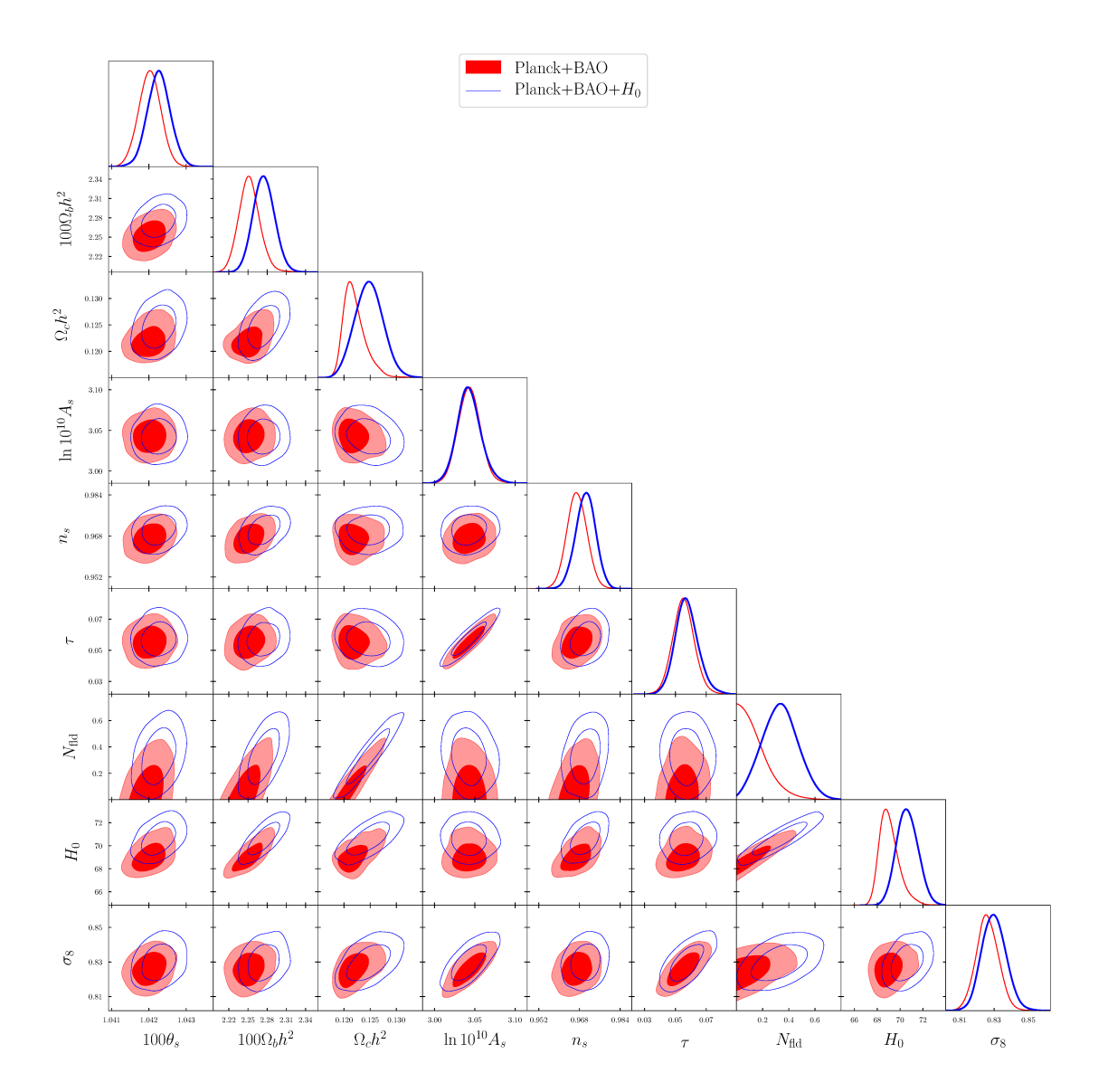


Figure 11. Posterior distributions for a model with  $N_{\text{eff}} = 3.046$  and varying  $N_{\text{fld}}$  for the *Planck* TT, TE, EE + BAO data set with (thin blue contours) and without an  $H_0$  prior (filled red regions). In both cases, the inner (outer) contours correspond to 68% (95%) confidence regions.

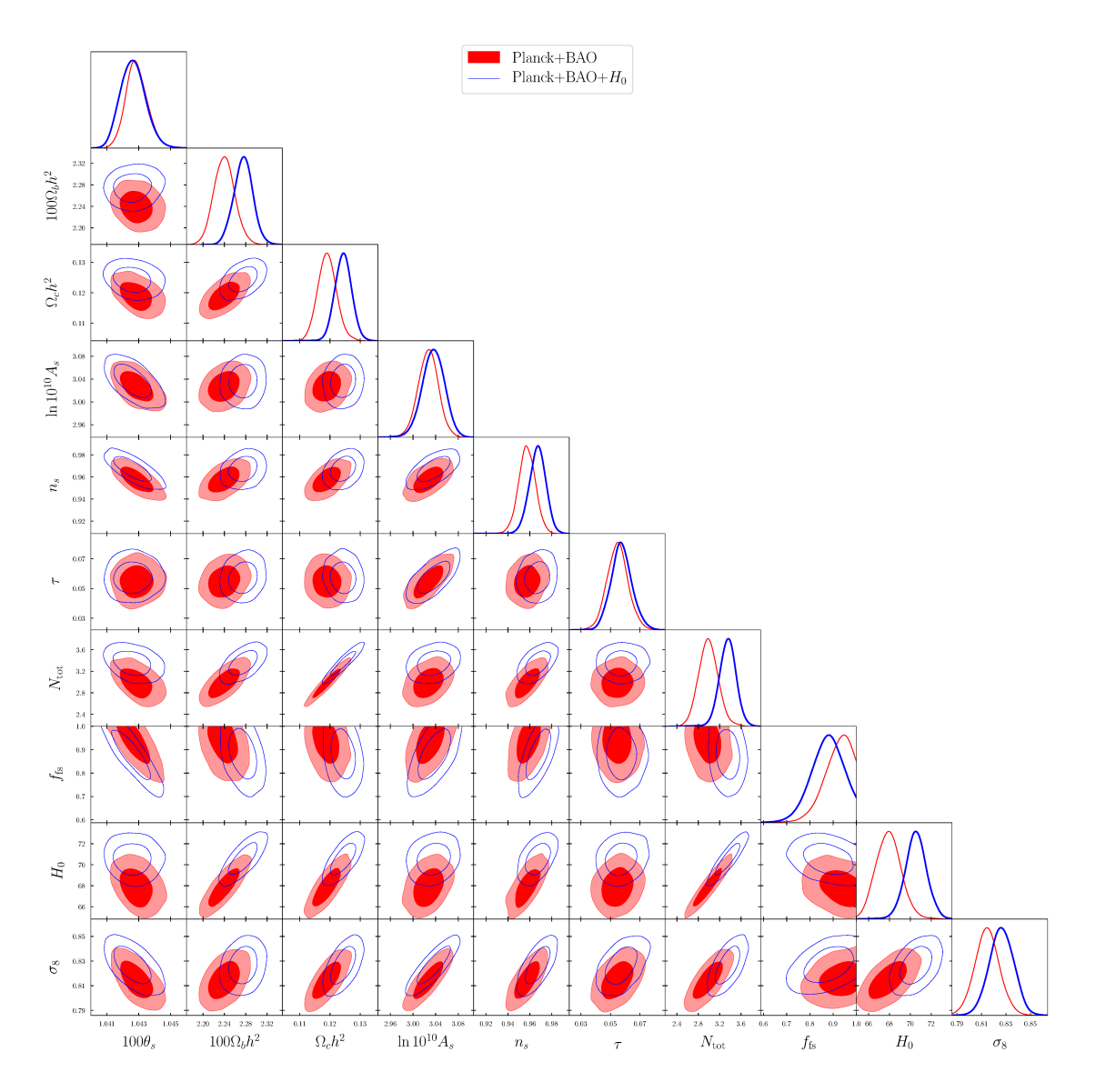


Figure 12. Posterior distributions for a model wit varying  $N_{\text{tot}}$  and  $f_{\text{fs}}$  for the *Planck* TT, TE, EE + BAO data set with (thin blue contours) and without an  $H_0$  prior (filled red regions). In both cases, the inner (outer) contours correspond to 68% (95%) confidence regions.

#### References

- [1] Planck collaboration, *Planck 2018 results. VI. Cosmological parameters*, arXiv:1807.06209 [INSPIRE].
- [2] K. Abazajian, G.M. Fuller and M. Patel, Sterile neutrino hot, warm, and cold dark matter, Phys. Rev. D 64 (2001) 023501 [astro-ph/0101524] [INSPIRE].
- [3] H. Vogel and J. Redondo, Dark radiation constraints on minicharged particles in models with a hidden photon, JCAP 02 (2014) 029 [arXiv:1311.2600] [INSPIRE].
- [4] A. Berlin and N. Blinov, Thermal dark matter below an MeV, Phys. Rev. Lett. 120 (2018) 021801 [arXiv:1706.07046] [INSPIRE].
- [5] J. Halverson and P. Langacker, *TASI lectures on remnants from the string landscape*, PoS(TASI2017)019 [arXiv:1801.03503] [INSPIRE].
- [6] D. Baumann, D. Green and B. Wallisch, New target for cosmic axion searches, Phys. Rev. Lett. 117 (2016) 171301 [arXiv:1604.08614] [INSPIRE].
- [7] S. Weinberg, Goldstone bosons as fractional cosmic neutrinos, Phys. Rev. Lett. 110 (2013) 241301 [arXiv:1305.1971] [INSPIRE].
- [8] M. Millea, L. Knox and B. Fields, New bounds for axions and axion-like particles with keV-GeV masses, Phys. Rev. D 92 (2015) 023010 [arXiv:1501.04097] [INSPIRE].
- [9] CMB-S4 collaboration, CMB-S4 science book, first edition, arXiv:1610.02743 [INSPIRE].
- [10] SIMONS OBSERVATORY collaboration, The Simons Observatory: science goals and forecasts, JCAP 02 (2019) 056 [arXiv:1808.07445] [INSPIRE].
- [11] S. Bashinsky and U. Seljak, Neutrino perturbations in CMB anisotropy and matter clustering, Phys. Rev. D 69 (2004) 083002 [astro-ph/0310198] [INSPIRE].
- [12] Z. Hou, R. Keisler, L. Knox, M. Millea and C. Reichardt, How massless neutrinos affect the Cosmic Microwave Background damping tail, Phys. Rev. D 87 (2013) 083008 [arXiv:1104.2333] [INSPIRE].
- [13] D. Baumann, D. Green, J. Meyers and B. Wallisch, *Phases of new physics in the CMB*, *JCAP* **01** (2016) 007 [arXiv:1508.06342] [INSPIRE].
- [14] A. Friedland, K.M. Zurek and S. Bashinsky, Constraining models of neutrino mass and neutrino interactions with the Planck satellite, arXiv:0704.3271 [INSPIRE].
- [15] B. Follin, L. Knox, M. Millea and Z. Pan, First detection of the acoustic oscillation phase shift expected from the cosmic neutrino background, Phys. Rev. Lett. 115 (2015) 091301 [arXiv:1503.07863] [INSPIRE].
- [16] A.G. Riess, S. Casertano, W. Yuan, L.M. Macri and D. Scolnic, Large Magellanic Cloud Cepheid standards provide a 1% foundation for the determination of the Hubble constant and stronger evidence for physics beyond ΛCDM, Astrophys. J. 876 (2019) 85 [arXiv:1903.07603] [INSPIRE].
- [17] K.C. Wong et al.,  $H0LiCOW\ XIII.\ A\ 2.4\%$  measurement of  $H_0$  from lensed quasars:  $5.3\sigma$  tension between early and late-Universe probes, arXiv:1907.04869 [INSPIRE].
- [18] DES collaboration, Dark Energy Survey year 1 results: a precise H0 estimate from DES Y1, BAO, and D/H data, Mon. Not. Roy. Astron. Soc. 480 (2018) 3879 [arXiv:1711.00403] [INSPIRE].
- [19] G.E. Addison, D.J. Watts, C.L. Bennett, M. Halpern, G. Hinshaw and J.L. Weiland, Elucidating ΛCDM: impact of baryon acoustic oscillation measurements on the Hubble constant discrepancy, Astrophys. J. 853 (2018) 119 [arXiv:1707.06547] [INSPIRE].

- [20] N. Schöneberg, J. Lesgourgues and D.C. Hooper, The BAO+BBN take on the Hubble tension, JCAP 10 (2019) 029 [arXiv:1907.11594] [INSPIRE].
- [21] W.L. Freedman et al., The Carnegie-Chicago Hubble program. VIII. An independent determination of the Hubble constant based on the tip of the red giant branch, arXiv:1907.05922 [INSPIRE].
- [22] J.L. Bernal, L. Verde and A.G. Riess, The trouble with  $H_0$ , JCAP 10 (2016) 019 [arXiv:1607.05617] [INSPIRE].
- [23] K. Aylor, M. Joy, L. Knox, M. Millea, S. Raghunathan and W.L.K. Wu, Sounds discordant: classical distance ladder & ΛCDM-based determinations of the cosmological sound horizon, Astrophys. J. 874 (2019) 4 [arXiv:1811.00537] [INSPIRE].
- [24] L. Knox and M. Millea, *Hubble constant hunter's guide*, *Phys. Rev. D* **101** (2020) 043533 [arXiv:1908.03663] [INSPIRE].
- [25] A.G. Riess et al., A 2.4% determination of the local value of the Hubble constant, Astrophys. J. 826 (2016) 56 [arXiv:1604.01424] [INSPIRE].
- [26] C.D. Kreisch, F.-Y. Cyr-Racine and O. Doré, *The neutrino puzzle: anomalies, interactions, and cosmological tensions, Phys. Rev. D* **101** (2020) 123505 [arXiv:1902.00534] [INSPIRE].
- [27] F. Forastieri, M. Lattanzi and P. Natoli, Cosmological constraints on neutrino self-interactions with a light mediator, Phys. Rev. D 100 (2019) 103526 [arXiv:1904.07810] [INSPIRE].
- [28] E. Di Valentino, C. Bøehm, E. Hivon and F.R. Bouchet, Reducing the  $H_0$  and  $\sigma_8$  tensions with dark matter-neutrino interactions, Phys. Rev. D 97 (2018) 043513 [arXiv:1710.02559] [INSPIRE].
- [29] S. Ghosh, R. Khatri and T.S. Roy, *Dark Neutrino interactions phase out the Hubble tension*, arXiv:1908.09843 [INSPIRE].
- [30] V. Poulin, P.D. Serpico and J. Lesgourgues, A fresh look at linear cosmological constraints on a decaying dark matter component, JCAP 08 (2016) 036 [arXiv:1606.02073] [INSPIRE].
- [31] V. Poulin, T.L. Smith, T. Karwal and M. Kamionkowski, Early dark energy can resolve the Hubble tension, Phys. Rev. Lett. 122 (2019) 221301 [arXiv:1811.04083] [INSPIRE].
- [32] V. Poulin, T.L. Smith, D. Grin, T. Karwal and M. Kamionkowski, Cosmological implications of ultralight axionlike fields, Phys. Rev. D 98 (2018) 083525 [arXiv:1806.10608] [INSPIRE].
- [33] P. Agrawal, F.-Y. Cyr-Racine, D. Pinner and L. Randall, Rock 'n' roll solutions to the Hubble tension, arXiv:1904.01016 [INSPIRE].
- [34] T.L. Smith, V. Poulin and M.A. Amin, Oscillating scalar fields and the Hubble tension: a resolution with novel signatures, Phys. Rev. D 101 (2020) 063523 [arXiv:1908.06995] [INSPIRE].
- [35] C. Brust, Y. Cui and K. Sigurdson, Cosmological constraints on interacting light particles, JCAP 08 (2017) 020 [arXiv:1703.10732] [INSPIRE].
- [36] DES collaboration, Dark Energy Survey year 1 results: cosmological constraints from galaxy clustering and weak lensing, Phys. Rev. D 98 (2018) 043526 [arXiv:1708.01530] [INSPIRE].
- [37] H. Hildebrandt et al., KiDS+VIKING-450: cosmic shear tomography with optical and infrared data, Astron. Astrophys. 633 (2020) A69 [arXiv:1812.06076] [INSPIRE].
- [38] DES collaboration, Cosmological constraints from multiple probes in the Dark Energy Survey, Phys. Rev. Lett. 122 (2019) 171301 [arXiv:1811.02375] [INSPIRE].
- [39] HSC collaboration, Cosmology from cosmic shear power spectra with Subaru Hyper Suprime-Cam first-year data, Publ. Astron. Soc. Jap. 71 (2019) 43 [arXiv:1809.09148] [INSPIRE].

- [40] D. Blas, J. Lesgourgues and T. Tram, The Cosmic Linear Anisotropy Solving System (CLASS) II: approximation schemes, JCAP 07 (2011) 034 [arXiv:1104.2933] [INSPIRE].
- [41] A. Lewis, A. Challinor and A. Lasenby, Efficient computation of CMB anisotropies in closed FRW models, Astrophys. J. 538 (2000) 473 [astro-ph/9911177] [INSPIRE].
- [42] Planck collaboration, *Planck 2018 results. V. CMB power spectra and likelihoods*, arXiv:1907.12875 [INSPIRE].
- [43] M. Escudero and S.J. Witte, A CMB search for the neutrino mass mechanism and its relation to the Hubble tension, Eur. Phys. J. C 80 (2020) 294 [arXiv:1909.04044] [INSPIRE].
- [44] G. Mangano, G. Miele, S. Pastor, T. Pinto, O. Pisanti and P.D. Serpico, *Relic neutrino decoupling including flavor oscillations*, *Nucl. Phys. B* **729** (2005) 221 [hep-ph/0506164] [INSPIRE].
- [45] E. Grohs, G.M. Fuller, C.T. Kishimoto, M.W. Paris and A. Vlasenko, Neutrino energy transport in weak decoupling and big bang nucleosynthesis, Phys. Rev. D 93 (2016) 083522 [arXiv:1512.02205] [INSPIRE].
- [46] P.F. de Salas and S. Pastor, Relic neutrino decoupling with flavour oscillations revisited, JCAP 07 (2016) 051 [arXiv:1606.06986] [INSPIRE].
- [47] K.S. Jeong and F. Takahashi, Self-interacting dark radiation, Phys. Lett. B 725 (2013) 134 [arXiv:1305.6521] [INSPIRE].
- [48] M.A. Buen-Abad, G. Marques-Tavares and M. Schmaltz, Non-Abelian dark matter and dark radiation, Phys. Rev. D 92 (2015) 023531 [arXiv:1505.03542] [INSPIRE].
- [49] J. Lesgourgues, G. Marques-Tavares and M. Schmaltz, Evidence for dark matter interactions in cosmological precision data?, JCAP 02 (2016) 037 [arXiv:1507.04351] [INSPIRE].
- [50] M.A. Buen-Abad, M. Schmaltz, J. Lesgourgues and T. Brinckmann, *Interacting dark sector and precision cosmology*, *JCAP* **01** (2018) 008 [arXiv:1708.09406] [INSPIRE].
- [51] Z. Chacko, L.J. Hall, T. Okui and S.J. Oliver, CMB signals of neutrino mass generation, Phys. Rev. D 70 (2004) 085008 [hep-ph/0312267] [INSPIRE].
- [52] Z. Chacko, L.J. Hall, S.J. Oliver and M. Perelstein, Late time neutrino masses, the LSND experiment and the cosmic microwave background, Phys. Rev. Lett. 94 (2005) 111801 [hep-ph/0405067] [INSPIRE].
- [53] A. Berlin and N. Blinov, Thermal neutrino portal to sub-MeV dark matter, Phys. Rev. D 99 (2019) 095030 [arXiv:1807.04282] [INSPIRE].
- [54] A. Berlin, N. Blinov and S.W. Li, Dark sector equilibration during nucleosynthesis, Phys. Rev. D 100 (2019) 015038 [arXiv:1904.04256] [INSPIRE].
- [55] S. Hannestad and G. Raffelt, Constraining invisible neutrino decays with the cosmic microwave background, Phys. Rev. D 72 (2005) 103514 [hep-ph/0509278] [INSPIRE].
- [56] F.-Y. Cyr-Racine and K. Sigurdson, Limits on neutrino-neutrino scattering in the early universe, Phys. Rev. D 90 (2014) 123533 [arXiv:1306.1536] [INSPIRE].
- [57] M. Archidiacono and S. Hannestad, *Updated constraints on non-standard neutrino interactions* from Planck, JCAP **07** (2014) 046 [arXiv:1311.3873] [INSPIRE].
- [58] I.M. Oldengott, C. Rampf and Y.Y.Y. Wong, Boltzmann hierarchy for interacting neutrinos I: formalism, JCAP 04 (2015) 016 [arXiv:1409.1577] [INSPIRE].
- [59] F. Forastieri, M. Lattanzi and P. Natoli, Constraints on secret neutrino interactions after Planck, JCAP 07 (2015) 014 [arXiv:1504.04999] [INSPIRE].
- [60] I.M. Oldengott, T. Tram, C. Rampf and Y.Y.Y. Wong, Interacting neutrinos in cosmology: exact description and constraints, JCAP 11 (2017) 027 [arXiv:1706.02123] [INSPIRE].

- [61] L. Lancaster, F.-Y. Cyr-Racine, L. Knox and Z. Pan, A tale of two modes: neutrino free-streaming in the early universe, JCAP 07 (2017) 033 [arXiv:1704.06657] [INSPIRE].
- [62] N. Blinov, K.J. Kelly, G.Z. Krnjaic and S.D. McDermott, Constraining the self-interacting neutrino interpretation of the Hubble tension, Phys. Rev. Lett. 123 (2019) 191102 [arXiv:1905.02727] [INSPIRE].
- [63] J.F. Beacom, N.F. Bell and S. Dodelson, Neutrinoless universe, Phys. Rev. Lett. 93 (2004) 121302 [astro-ph/0404585] [INSPIRE].
- [64] G. Choi, C.-T. Chiang and M. LoVerde, Probing decoupling in dark sectors with the Cosmic Microwave Background, JCAP 06 (2018) 044 [arXiv:1804.10180] [INSPIRE].
- [65] C.-P. Ma and E. Bertschinger, Cosmological perturbation theory in the synchronous and conformal Newtonian gauges, Astrophys. J. 455 (1995) 7 [astro-ph/9506072] [INSPIRE].
- [66] W. Hu, Covariant linear perturbation formalism, ICTP Lect. Notes Ser. 14 (2003) 145 [astro-ph/0402060] [INSPIRE].
- [67] J.R. Bond and A.S. Szalay, The collisionless damping of density fluctuations in an expanding universe, Astrophys. J. 274 (1983) 443 [INSPIRE].
- [68] W. Hu and N. Sugiyama, Anisotropies in the cosmic microwave background: an analytic approach, Astrophys. J. 444 (1995) 489 [astro-ph/9407093] [INSPIRE].
- [69] M. Zaldarriaga and D.D. Harari, Analytic approach to the polarization of the cosmic microwave background in flat and open universes, Phys. Rev. D 52 (1995) 3276 [astro-ph/9504085] [INSPIRE].
- [70] W. Hu and M.J. White, The damping tail of CMB anisotropies, Astrophys. J. 479 (1997) 568 [astro-ph/9609079] [INSPIRE].
- [71] W. Hu, M. Fukugita, M. Zaldarriaga and M. Tegmark, CMB observables and their cosmological implications, Astrophys. J. 549 (2001) 669 [astro-ph/0006436] [INSPIRE].
- [72] W. Hu and N. Sugiyama, Small scale cosmological perturbations: an analytic approach, Astrophys. J. 471 (1996) 542 [astro-ph/9510117] [INSPIRE].
- [73] T. Brinckmann and J. Lesgourgues, MontePython 3: boosted MCMC sampler and other features, Phys. Dark Univ. 24 (2019) 100260 [arXiv:1804.07261] [INSPIRE].
- [74] BOSS collaboration, The clustering of galaxies in the completed SDSS-III Baryon Oscillation Spectroscopic Survey: cosmological analysis of the DR12 galaxy sample, Mon. Not. Roy. Astron. Soc. 470 (2017) 2617 [arXiv:1607.03155] [INSPIRE].
- [75] F. Beutler et al., The 6dF Galaxy Survey: Baryon Acoustic Oscillations and the local Hubble constant, Mon. Not. Roy. Astron. Soc. 416 (2011) 3017 [arXiv:1106.3366] [INSPIRE].
- [76] A.J. Ross, L. Samushia, C. Howlett, W.J. Percival, A. Burden and M. Manera, The clustering of the SDSS DR7 main Galaxy sample I. A 4 per cent distance measure at z = 0.15, Mon. Not. Roy. Astron. Soc. 449 (2015) 835 [arXiv:1409.3242] [INSPIRE].
- [77] A. Gelman and D.B. Rubin, Inference from iterative simulation using multiple sequences, Statist. Sci. 7 (1992) 457.
- [78] S.P. Brooks and A. Gelman, General methods for monitoring convergence of iterative simulations, J. Comput. Graph. Stat. 7 (1998) 434.
- [79] P. Virtanen et al., SciPy 1.0: fundamental algorithms for scientific computing in Python, Nature Meth. 17 (2020) 261.
- [80] iminuit team, iminuit A Python interface to minuit, https://github.com/scikit-hep/iminuit.
- [81] F. James and M. Roos, Minuit A system for function minimization and analysis of the parameter errors and correlations, Comput. Phys. Commun. 10 (1975) 343.

- [82] Planck collaboration, *Planck 2015 results. XIII. Cosmological parameters*, *Astron. Astrophys.* **594** (2016) A13 [arXiv:1502.01589] [INSPIRE].
- [83] E. Aver, K.A. Olive and E.D. Skillman, The effects of He I λ10830 on helium abundance determinations, JCAP 07 (2015) 011 [arXiv:1503.08146] [INSPIRE].
- [84] A. Lewis, GetDist: a Python package for analysing Monte Carlo samples, arXiv:1910.13970 [INSPIRE].